NTNU
Norwegian University of
Science and Technology

Multiband UWB Antenna design for WiFi, LTE and 5G

Håvard Grundtvig Dahle Løvaas

Master of Science in Electronics
Submission date: June 2017
Supervisor: Egil Eide, IES

Norwegian University of Science and Technology
Department of Electronic Systems

Problem description

The purpose of this thesis is to design and test an Ultra-Wide-Band omni-directional antenna for LTE and Wi-Fi. An UWB antenna should have constant gain and beamwidth over the frequency band. A literature study on the state-of-art on UWB antennas will form the basis for this thesis and the choice of design. The antenna will be designed and simulated in CST, and later tested in an anechoic chamber. The antenna should at least operate on frequencies from $800\,\mathrm{MHz}$ to $2.6\,\mathrm{GHz}$, but a wider band including higher frequencies might be necessary to support other wireless applications.

Abstract

In this thesis, a new design of an ultra-wideband planar slot antenna is presented. The antenna is made on FR4 and the design is compact with a size of $109.2\,\mathrm{mm} \times 156\,\mathrm{mm}$. The bandwidth of the antenna was measured to be $7.5\,\mathrm{GHz}$ ranging from $1.2\,\mathrm{GHz}$ to $8.7\,\mathrm{GHz}$ when only analyzing the S-parameters. The antenna is installed with a reflector plate at the distance of $30\,\mathrm{mm}$ which increases the directivity of the antenna and increases the antenna gain. The bandwidth according to $S_{1,1}$ is from $560\,\mathrm{MHz}$ to $8.7\,\mathrm{GHz}$ when the reflector plate is removed. The antenna was first designed and simulated in CST and later produced and measured in an antenna lab at NTNU. The antenna is linear horizontal polarized and the beam pattern have a wide beam up to 60° in the E-plane and E-plane for frequencies under $2.5\,\mathrm{GHz}$. In simulations, an absorbent was added to improve the beam patterns for the antenna. The absorbent was not added to the produced antenna that was measured.

Sammendrag

I denne masteroppgaven har det blitt designet en ultrabredbånds planar antenne med båndbredde på $7.5\,\mathrm{GHz}$. Antennen er produsert på FR4 og har en størrelse på $109.2\,\mathrm{mm}\times156\,\mathrm{mm}$ Antennen opererer på frekvensene fra $1.2\,\mathrm{GHz}$ og opp til $8.7\,\mathrm{GHz}$ når den er montert med avstand på $30\,\mathrm{mm}$ til en reflektorplate. Reflektorplaten gjør at antennen stråler mer i positiv z-retning og øker antennens forsterkning. Uten reflektorplaten har antennen en båndbredde, ved å analysere $S_{1,1}$ fra $560\,\mathrm{MHz}$ og opp til $8.7\,\mathrm{GHz}$. Antennen er lineær polarisert i horisontal retning og har en strålebredde på over 60° for frekvenser under $2.5\,\mathrm{GHz}$. Antennen ble først simulert i CST og senere produsert og testet med nettverksanalysator og i et antennekammer ved NTNU. Ved simulering ble forskjellige teknikker for å minimere rippel i strålingsdiagrammene ved frekvenser over $2.5\,\mathrm{GHz}$ gjennomført, og dette gav gode resultater. En av teknikkene var å legge en absorbent langs flere av kantene på antennen, men dette ble ikke gjort på den produserte antennen. Dette kunne muligens ha bedret de målte strålingsdiagrammene.

Preface

This thesis concludes my Master of Science education at the Norwegian University of Science and Technology (NTNU) in Trondheim. The thesis was performed throughout the spring in 2017 at the department of Electronic Systems.

I want to thank NTNU and the Department of Electronic Systems for letting me work with such an interesting subject and to let me use the equipment and the facilities at the University. A big thank you to the Elpro lab and Senior Engineer Terje Mathiesen at NTNU for printing my design and assisting me with guidelines and equipment when needed. My supervisor Egil Eide has also helped me a lot and guided me in the design process and showed me different techniques and been a good person to discuss different topics with. I'm also grateful for the help from Tele Engineering workshop at NTNU for constructing the reflector plate and divinycell plate for my design.

Trondheim, 23 June 2017

Håvard Grundtvig Dahle Løvaas

Table of Contents

List of Figures

Abbreviations

ANA Automatic Network Analyzer

AUT Antenna under Test

CST Computer Simulation Technology

LTE Long Time Evolution

MIMO Multiple input multiple output

OFDM Orthogonal Frequency Division Multiplexing

PEC Perfect Electric Conductor

S-Parameter Scattering Parameter

UWB Ultra-Wideband

Chapter 1

Introduction

This thesis is a part of an ongoing project at NTNU. The project investigates the possibility to utilize massive MIMO in a maritime environment to increase the link capacity and range. The project will focus on Wi-Fi, LTE and some possible 5G-bands and an UWB antenna is an important component in such a system. The purpose of this thesis is to form an antenna design that could be sufficient for this project and to suggest a design for the massive MIMO base station.

Ultra-Wideband (UWB) antennas are today used in wideband communication and in radar imaging and have received a growing interest the recent years. Wideband communication might be a solution to the higher demand of capacity to multiple devices and UWB antenna is a key component in a UWB communication system. Wideband antennas are also convenient as test antennas since they can be used at multiple frequencies to test different applications. Even though UWB technology have received growing attention the last few decades, UWB antennas can be traced back to Oliver Lodge's experiments on "Syntony" in 1898 (Lodge, 1898). His hypothesis was that the transmitting and receiving antenna should be tuned to the same frequency to improve the received power. In his patent drawings from 1898 he introduced the bow-tie and later the spherical antenna. With the development in television and radio broadcasting the demand of antennas operating at a wider band of frequencies has been growing. Many of these antennas were operating at multiple narrow band channels in a wide

range. (Schantz, 2004) When we discuss UWB today we often refer to an antenna which will be constant in gain, impedance, phase in the whole frequency band to support wideband channels without distorting the received signal. Some modulations like Orthogonal Frequency Division Multiplexing (OFDM) or a multi-band approach might not be sensitive to variations in the frequency band. (Schantz, 2003)

The thesis starts with a presentation of the project and its requirements and followed by a presentation of the literature review that was performed in the start of this thesis. Chapter 4 will present some theory for this thesis and chapter 5 will describe the design approach and present results from simulations. Chapter 6 presents the experimental results obtained through the project and chapter 7 will contain a discussion. The last chapter will be the conclusion and finish of this thesis.

Chapter 2

Requirements

This chapter will provide the requirements and specifications for this master thesis. The purpose of this thesis is to design an antenna for massive Multiple input multiple output (MIMO) testing for Wi-Fi, LTE and 5G in a maritime environment. LTE, Wi-Fi and 5G will operate at different frequencies and a UWB antenna will be a key component in this setup. The massive MIMO rack will be a cylinder with multiple panels with multiple antennas around the cylinder as shown in figure 2.1. It is often desired to keep the design small and compact, and that is one of the requirements for this design. The key requirements are listed in the table 2.1 beneath.

Table 2.1: Requirements

Frequency	$800\,\mathrm{MHz}$ to $6\,\mathrm{GHz}$	LTE, Wi-Fi and 5G
Horizontal-Plane	0 to $360°$	For the cylinder
Horizontal-Beamwidth	$\approx 60°$	For one panel
Vertical-Plane	$+/- 27°$	
Size cylinder	r $= 30\,\mathrm{cm}$, h $= 30\,\mathrm{cm}$	r = radius, h = height
Polarization	Single linear polarization	
Design	Planar and compact	
$S_{1,1}$	Below $-10\,\mathrm{dB}$	In the bandwidth
Gain	No requirements	

The size of the cylinder is not exact but should be approximately as described in table 2.1. The cylinder will consist of multiple panels with as many antennas at each panel as possible. If the cylinder should consist of

16 panels and be at the size from the specifications, each panel should be at the size of $12\,\mathrm{cm} \times 30\,\mathrm{cm}$. In the proposed design the beam can be steared by switching between the panels and possibly 1 or more panels will cooperate by utilizing the massive MIMO benefits.

The construction of the base station has to be quite robust and should tolerate the harsh environment and strong forces that can be experienced at sea. This thesis will not consider the construction part of the cylinder and primarily focus on the antenna design.

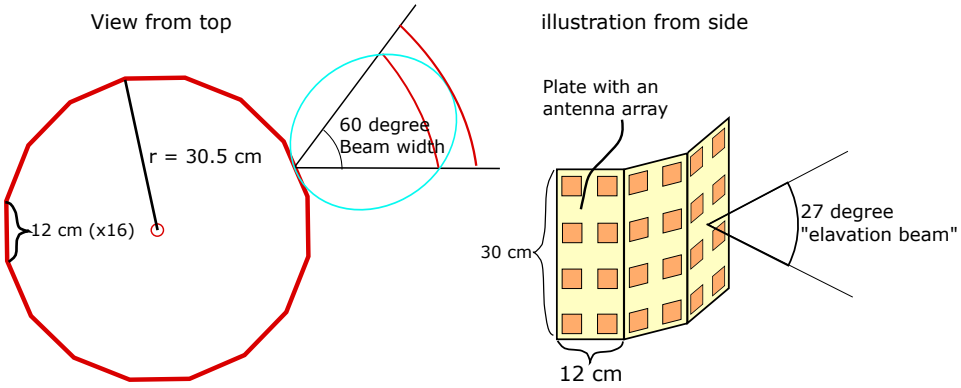

Figure 2.1: Illustration of the cylinder with multiple panels and multiple antennas

Chapter 3

Literature Review

A thorough literature review was completed to get an understanding on the state-of-art in the field of UWB antennas and antenna design. Papers on UWB patch and slot antennas was the primary focus in this literature review. There are a lot of UWB antenna designs and the idea was to find a design that with some modifications and tuning would fulfill the specifications for this project. The paper with the most promising design that provided a starting point for the design formed by this master thesis was from the paper "A Novel Ultra-Wideband Planar Slot Antenna" (Wang and Yu, 2010). This antenna had the larges bandwidth of all the planar antennas found in this thesis, and was compact and showed good promise as a start design for this thesis.

A lot of sufficient UWB antenna designs were found including the Vivaldi-antenna, Log-periodic, different horn-antennas, sinusoidal antenna and a lot of PCB-antennas with different shapes. Most of these antennas are not planar and were not considered for this thesis. At this stage the primary focus was to find an antenna that was compact, planar and with the UWB properties. When a promising design was found, it was modelled and simulated in CST Studie Suite. CST is a powerful three-dimensional electromagnetic modelling and simulation tool where different electromagnetic devices can be simulated at multiple frequencies. It was convenient to simulate different designs to see if the design had the right properties and

could be a starting point for this thesis. A total of about 15 designs were modelled and simulated, and the simulations were very useful to give a clue on the properties of the design.

3.1 A Novel Ultra-Wideband Planar Slot Antenna

The most promising designs from the literature review was recreated and simulated in CST and is shown in figure 3.1. The different designs were then compared on frequency span by comparing S-parameters. The design formed in this thesis should have a bandwidth ranging from $800\,\mathrm{MHz}$ to $6\,\mathrm{GHz}$, which in S parameters translates to a $S_{1,1} \leq -10\mathrm{dB}$ for the given frequency band. Most of the designs that were simulated had a frequency span at higher frequencies than the specifications for this project. The designs were also compared on far field plots, of both E-plane and H-plane, and size. The most promising design was discovered in the paper: "A Novel Ultra-Wideband Planar Slot Antenna" (Wang and Yu, 2010). The most difficult part was to find a planar design with large enough bandwidth. The design that formed the starting point had a bandwidth ranging from $2.8\,\mathrm{GHz}$ to $32\,\mathrm{GHz}$.

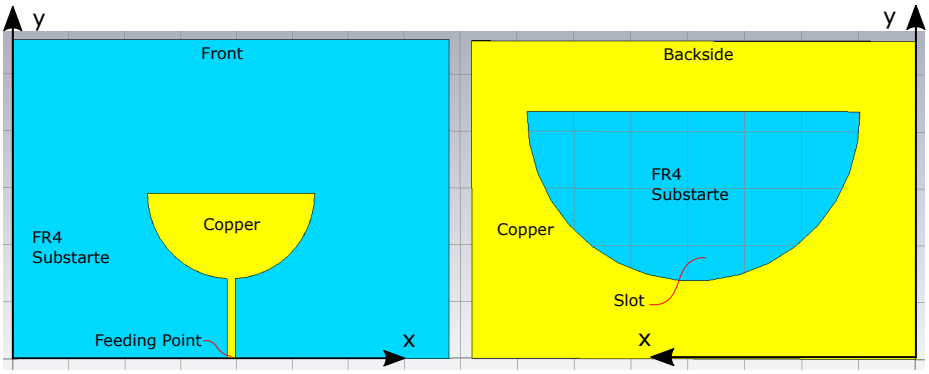

Figure 3.1: Front and backside of the antenna form (Wang and Yu, 2010)

Chapter 4

Background

This chapter will present some relevant theory for this thesis including basic antenna theory, array and massive MIMO theory and theory on different measurement techniques and the most important parameters used in this thesis.

4.1 Patch and slot antenna

Microstrip antennas are popular due to their size, cost of manufacturing, ease of installation and robustness. They are made with modern printed-circuit technology and design as printed-circuit boards. Patch antennas have been found since 1953 but became popular in the 1970s. Both patch and slot antennas can be made with this technology and often consists of a substrate with a thin layer of copper on both sides. Each side of the structure can be designed in various ways to give the antenna different properties. Patch antennas are often narrow banded, and slot antennas are often more wide band. The slot can be made on the ground side of the substrate and are often excited by a structure on the opposite side. This can be a transmission line, patch structure or any structure. The main concerns regarding patch antennas are low efficiency, narrow frequency bandwidth, low power and poor polarization purity. (Balanis, 2005)

4.1.1 Babinet's principle

Babinet's principle is used to describe the fields and impedance of a slot antenna. As illustrated in fig 4.1 a complementary antenna, in metal, can be made at the same size as the slot. By analyzing the complementary antenna and its field we can also describe the slot antennas field by applying Babinet's principle. The first rule is a description of the impedance of the slot antenna Z_s in relation to the impedance of the complementary antenna Z_d.

$$Z_s \times Z_d = \frac{\eta^2}{4}$$

$$\text{where, } \eta = \sqrt{\frac{\mu}{\epsilon}}$$

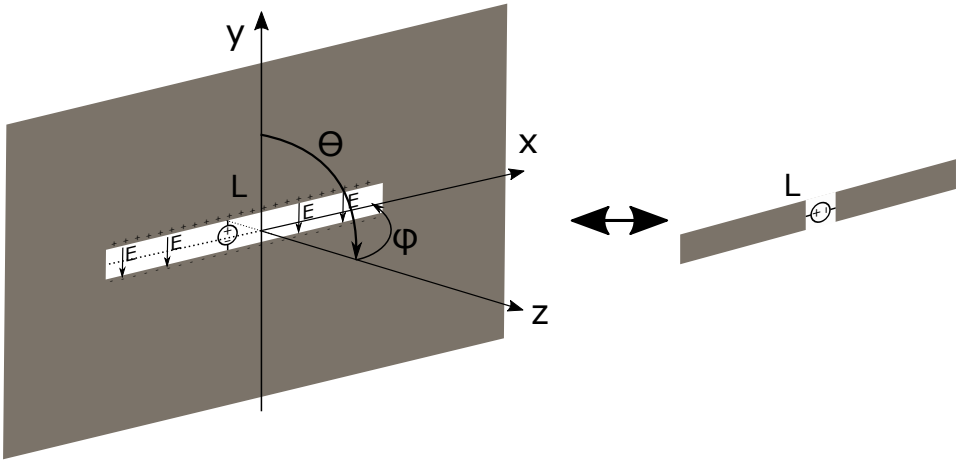

Figure 4.1: complementary antennas - A slot antenna is illustrated to the left and its complementary antenna (dipole) to the right

The second relation between the complementary antennas is a relation between the E- and H-plane of the two antennas.

$$E_{\theta s} = H_{\theta s}$$

$$E_{\phi s} = H_{\phi s}$$

$$H_{\theta s} = \frac{-E_{\theta s}}{\eta^2}$$

$$H_{\theta s} = \frac{-E_{\phi s}}{\eta^2}$$

The dipole antenna is a well-known antenna with well-defined fields and properties. Babinet's principle makes it possible to compare a slot antenna to a known structure. The polarization is changed, the dipole to the right is horizontal polarized and by applying Babinet's principle we know that the slot antenna must be vertically polarized.

4.2 Array

Antenna arrays are widely used in many applications and are used in radar technology, radio astronomy and are also common in cellular networks like Long Time Evolution (LTE). The main advantages with antenna arrays are increase in directivity, the possibility to control the shape of radiation pattern and to steer the main lobe. An array can consist of 2 or hundreds of elements. Distance between the elements and phase difference between the excited signal is the most important parameters that affect the properties and radiation pattern of the array. The total pattern can be divided in an element factor, which is the beam pattern of the antenna the array consists of, and an array factor which is a pattern that is calculated by knowing the number of elements in the array and the phase difference of the excited signal to the elements. A classic broadside array will have no phase difference between the antennas and a distance between the elements of less than $\frac{5*\lambda}{6}$. The directivity of the array will then be approximately $2N\frac{d}{\lambda}$ where d is the element distance, λ is the wavelength and N is the number of elements in the array.

4.3 Massive MIMO

Massive multiple-input multiple-output (Massive MIMO) is the concept of using multiple antennas at both transmitter and possibly at the receiver to enhance the capacity of the link by utilizing the multipath propagation. MIMO has been around for decades and is found in many wireless systems like Wi-Fi, 3G and Long Term Evolution (LTE). LTE base stations are typically equipped with 4 (2x2) or 8 (4x2) antennas, but massive MIMO is a large antenna array of hundred antennas, or more, potentially serving

tens of terminals simultaneously. (E. G. Larsson, Tufvesson, and Marzetta, 2014) The main improvement from massive MIMO is the increase in spectral efficiency. Spectrum is a limited and expensive resource and better exploitation of this resource sending more bits per second per hertz. (Løvaas, 2016)

4.4 Measurements and parameters

This section will briefly explain the parameters that are important in antenna design and measurement. This section will also include a description on how some of these parameters are measured.

4.4.1 S-parameter

Scattering Parameter (S-Parameter) is a parameter that is useful to analyze the electrical behavior of an antennas and circuits. S-parameters can be used for a system with multiple ports and describes the electrical behavior between the different ports by a matrix of s-parameters. A circuit with N ports will have a matrix of N^2 s-parameters. If there is only one port a 1×1-Matrix is made with a parameter named $S_{1,1}$ which denotes how much power that is reflected by the circuit or device that port 1 is connected to. In antenna design a low $S_{1,1}$ translate to an antenna that radiates most of the power that is applied to the antenna. If $S_{1,1}$ is lower than $-10\,\mathrm{dB}$ the antenna radiates at least 90 % of the power that is applied to it. $S_{1,1}$ lower than $-10\,\mathrm{dB}$ is often a minimum limit in antenna design and in UWB antenna design the bandwidth is often the frequency range that has a $S_{1,1}$ below $-10\,\mathrm{dB}$. A system with 2 ports will generate a 2×2-Matrix of s-parameters where $S_{2,1}$ and $S_{1,2}$ tells how much power that is transferred from one port to the other. If the two ports are connected to two antennas the $S_{2,1}$ and $S_{1,2}$ should be low because it is desired to have a minimum of coupling between the antennas in an array. S-parameters can also give information on phase changes and impedance in the circuit, but in antenna design the main reason to analyze the s-parameter is to know the gain and losses of the antenna, and to find out if the antenna radiates the power applied to the antenna.

4.4.2 Directivity

Directivity is a measure of the antennas ability to focus its energy and beam in a direction. It is often measured in dBi and is relative to an isotropic antenna which radiates equally in all directions. Increased directivity will improve the gain of an antenna and will increase the range of a communication system if the antenna is pointed correctly to the receiving or transmitting antenna.

4.4.3 Far field

An antenna generates a near field and a far field. The far field is when the electromagnetic wave consists of plane E- and H-field that are perpendicular to each other. The fields will not change but will be attenuated by the distance R with a factor of 1/R. The far field starts at around $\frac{2D^2}{\lambda}$ and D is the largest length/dimension of the transmitting antenna.

4.4.4 Antenna Measurements

By connecting the Antenna under Test (AUT) to an Automatic Network Analyzer (ANA) it is not complicated to measure s-parameters and impedance for the antenna. Measurements of the patterns of the antenna can be performed in an anechoic chamber. Figure 4.2 illustrates an anechoic chamber similar to the one available at NTNU. The walls inside the chamber is covered with pyramid shaped absorbents that will absorb the energy from the signals and not reflect and distort the results. The transmitting antenna is a directive horn antenna that is controlled from a computer connected to an ANA. The AUT is connected to the second port of the ANA and $S_{1,2}$ is the parameter that is analyzed to get a plot of the beam pattern. To get a 360° pattern the AUT is installed on a rotating platform and controlled by a motion controller (MM4005 in figure 4.2) and all the equipment is controlled by a computer with a MatLab-script.

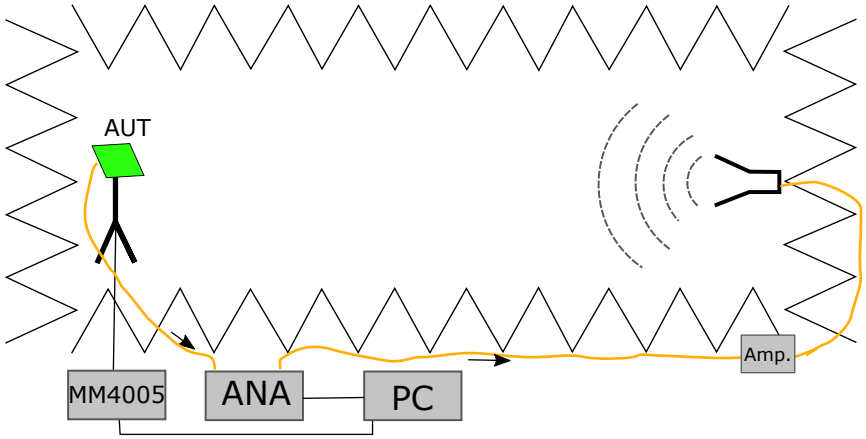

Figure 4.2: Illustration of a typical setup for an anechoic chamber similar to the one at NTNU.

4.5 Wheeler radiansphere and small antennas

Electrically-small antennas are antennas that fits inside a radiansphere with a radius of:

$$a = \frac{1}{k}, \text{ where } k = \frac{2\pi}{\lambda} \; (Wheeler,\ 1959)$$

From Wheelers paper on small antennas he presents some properties and relations between size, efficiency and bandwidth for small antennas. These studies were later reexamined by Lan Jen Chu, Roger Harrington and Mclean. From Wheelers studies the formula beneath were formed linking bandwidth, size and quality-factor together. Q-factor is a dimensionless factor that describes the stored energy and the dampening in a resonator. A resonator with high Q-factor has low dampening and low rate of energy loss.

$$\frac{f_{max} - f_{min}}{f_{center}} = k^3 a^2 = \frac{1}{Q}, \text{ where Q is Q-factor}$$

4.6 CST

CST is a powerful three-dimensional electromagnetic modelling and simulation tool where different electromagnetic devices can be simulated at a large span of frequencies. Simulations with CST may include mechanical and thermal effects. CST is useful in the development of an antenna

and gives a good picture of the performance and properties of any antenna design. H-fields, E-fields, surface currents, efficiency, S-parameters and impedance are some of the useful parameters that can be produced by CST.

Chapter 5

Method and Simulation Results

This chapter will provide a step-by-step review of the design process and show simulations from CST and why different changes and adjustments were done. As covered in chapter 2 a thorough literature review formed the basis for the design. The purpose of this chapter is to show the steps from the starting point to the final design. A lot of different techniques were tested, but this review only shows the steps that were included in the final design. First a single antenna was designed and optimized for the specifications presented in table 2.1. The orientations of the planes are shown in figure 5.1 and is the orientation that is used throughout this chapter.

5.1 Starting point

The design from (Wang and Yu, 2010) was created in CST as described in section 3.1. The antenna operates as a monopole at lower frequencies and as a traveling wave antenna at higher frequencies. The half circle structure has a length of $10\,\mathrm{mm}$ and will operate as a monopole for frequencies up to approximately $7.5\,\mathrm{GHz}$ and as a travelling wave antenna for the frequencies above. $15\,\mathrm{GHz}$ is the center frequency for the antenna that was found in (Wang and Yu, 2010). The wave travels up the feed and spread on each edge of the half circle. There is coupling to the slot on the backside and the wave also travels along the edge of the bigger half circle towards the top of the antenna.

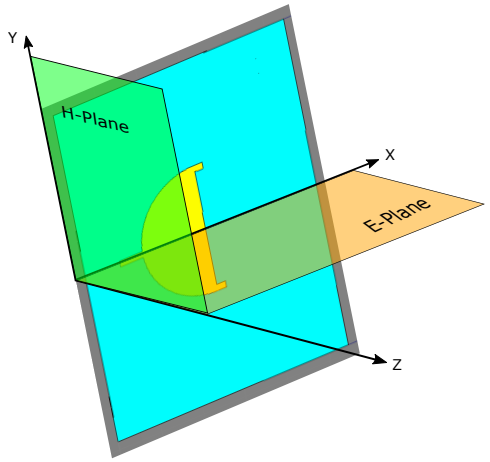

Figure 5.1: Illustration of the orientation of E-plane and H-plane

The design shown in figure 3.1 is a recreated design of the antenna from (Wang and Yu, 2010) with a few modifications. The design from (Wang and Yu, 2010) had a size of $70\,\mathrm{mm} \times 70\,\mathrm{mm}$ with a long feed. The recreated design was $8\,\mathrm{mm}$ shorter to reduce the size. The plot of $S_{1,1}$ in figure 5.2 shows great promise, but should be under $-10\,\mathrm{dB}$ from $2.3\,\mathrm{GHz}$.

5.2 Scaling

The initial design had frequency that spanned from $2.3\,\mathrm{GHz}$ and up to frequencies much higher than required. The first step of modification was to make the design larger and scale the almost every dimension by a factor of 2.6. All dimensions where scaled by this factor without the width of the feed transmission line. The feed must be equal to a $50\,\Omega$ transmission line and should not be scaled in width, but the length can be modified. A up scaling by a factor of 2.6 would theoretically lower f_{min} and f_{max} by the same factor ($f_{min} = 0.884\,\mathrm{GHz}$ and $f_{max} = 12.3\,\mathrm{GHz}$). The monopole behavior will be for lower frequencies and the antenna will start to operate as a travelling wave antenna for frequencies above approximately $2.8\,\mathrm{GHz}$. As shown figure 5.3 the frequency got lower and the values of $S_{1,1}$ is lower which translates to more power radiated from the antenna. The bandwidth is at this point from $1.45\,\mathrm{GHz}$ to $7.45\,\mathrm{GHz}$. The design was scaled by a larger factor and had a bandwidth from $800\,\mathrm{MHz}$ as specified, but the

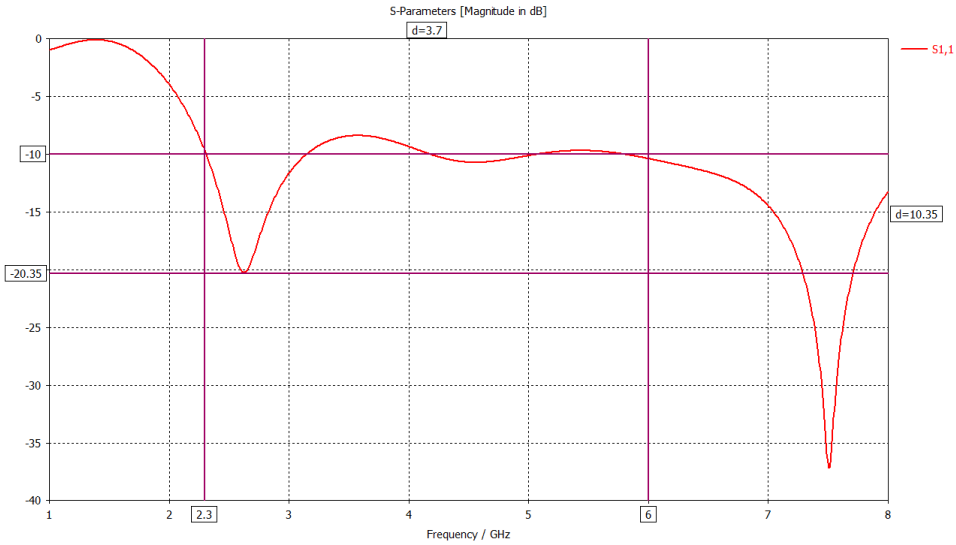

Figure 5.2: $S_{1,1}$ for the recreated design from (Wang and Yu, 2010) simulated in CST

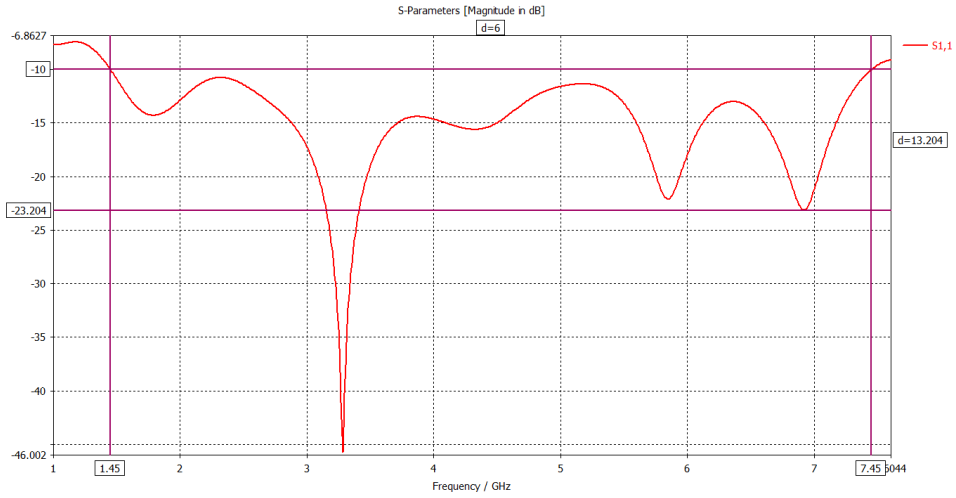

Figure 5.3: $S_{1,1}$ for the scaled design from (Wang and Yu, 2010) simulated in CST

overall size got too big for this project and it was decided to keep it at the scaling of 2.6 to keep the size compact and possible to manufacture with the available equipment at NTNU.

5.3 Reflector plane

A $125\,\mathrm{mm} \times 400\,\mathrm{mm}$ reflector plane was added at a distance h from the antenna to reflect the radiated power in one direction. The distance was at first set to $\lambda_{max}/2$. The half wavelength for the highest frequency (f_{max} = $6\,\mathrm{GHz}$) is equal to $25\,\mathrm{mm}$. From a parameter sweep the distance was later set to $27\,\mathrm{mm}$ due to better performance on the plots of E-plane and H-plane and more ideal S-parameters. To be able to mount the antenna at $27\,\mathrm{mm}$ from the reflector plate, a plate of divinycell was placed in between the reflector and the antenna as shown in figure 5.4. Divinycell is a material with low dielectric constant and should not affect the results and performance of the antenna. Divinycell is applied to the simulations further through the design process. The antenna, reflector plate and divinycell plate could be glued or screwed together when produced.

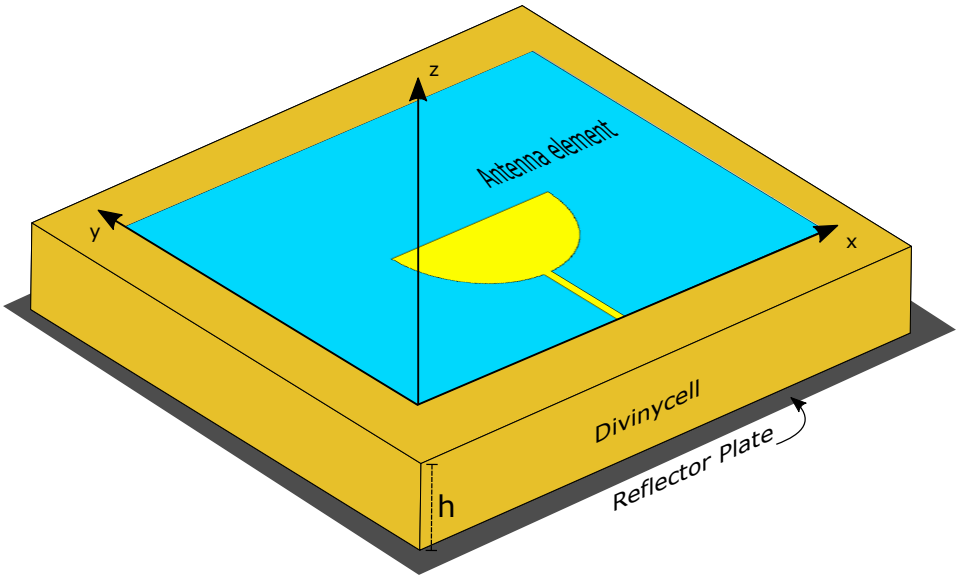

Figure 5.4: Illustration of the assembly of the antenna, divinycell-plate and reflector plate

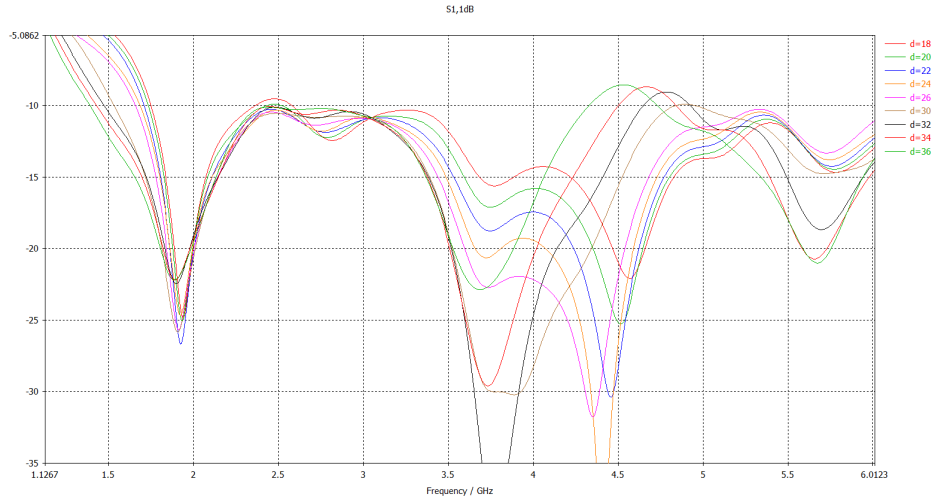

Figure 5.5: $S_{1,1}$ for different values of h simulated in CST

In fig 5.5 it is illustrated that the distance can range from $22\,\mathrm{mm}$ to $30\,\mathrm{mm}$. Out of this range $S_{1,1}$ would be greater than $-10\,\mathrm{dB}$ at $4.5\,\mathrm{GHz}$ which is unwanted. As shown in figure 5.6 and figure 5.7 the beam is more directional in one direction in the simulations including the reflector plane. The same characteristics was shown in all plots of the E-plane and H-plane at higher frequencies as well. The reflector plate could be placed at both sides of the antenna, but was placed on the slot side. This was wanted because the antenna was to be feed from this side, and it was convenient to have the feed and the reflector on the same side of the design.

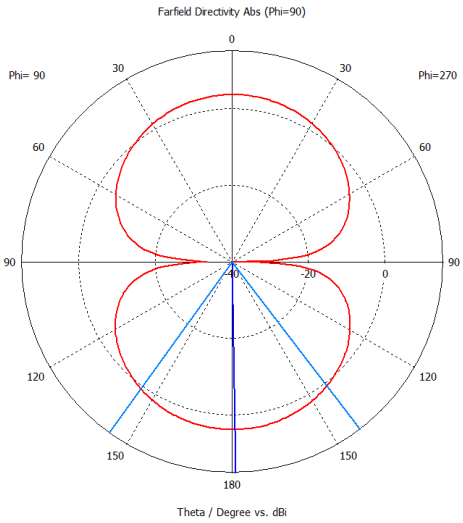

(a) Without reflector

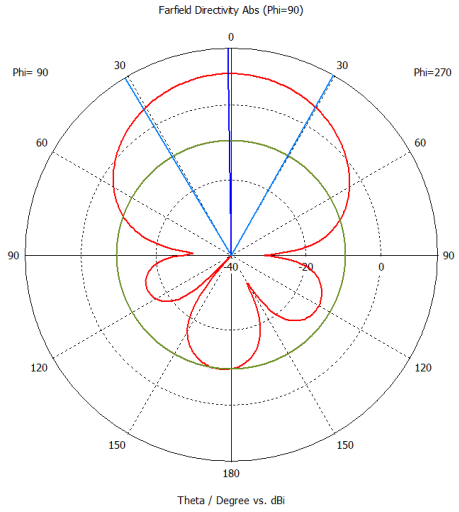

(b) With reflector at h = 27 mm

Figure 5.6: H-plane at 1.5 GHz simulated in CST

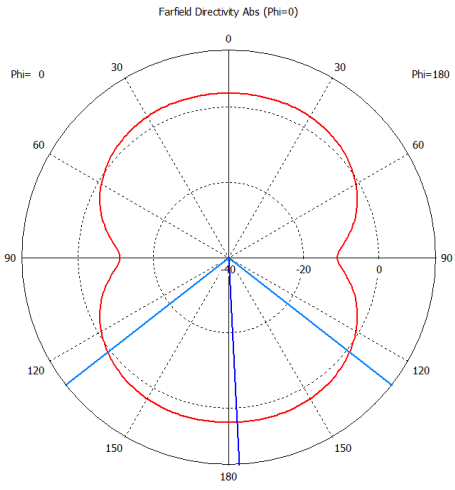

(a) Without reflector

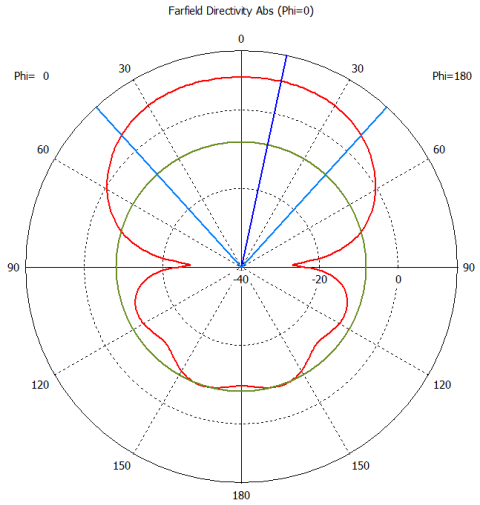

(b) With reflector at h = 27 mm

Figure 5.7: E-plane at 1.5 GHz simulated in CST

5.4 Improving the E-plane and H-plane

The radiation patterns for both H-plane and E-plane had a lot of ripple at frequencies above $2.5\,\mathrm{GHz}$ and needed some improvement. A technique where horns or taps are added at both sides gave good results for the E-plane and H-plane. This technique was found through the literature review in (Aziz and Jamlos, 2016) and (Tammam et al., 2012). The added taps are illustrated in figure 5.8. The taps will adds a notch to the design that will prevent some of the surface current to spread out on the upper edge of the slot and on the upper edge of the feed. In figure 5.9 a plot of the surface current at $6\,\mathrm{GHz}$ is illustrated. The black arrows illustrates the expected and preferred direction for the travelling wave. The red arrows in figure 5.9 shows the unwanted surface currents that possibly creates a deep notch and ripple in the radiation patterns at frequencies higher than $2.5\,\mathrm{GHz}$. To suppress these currents an absorbing material is added that attenuate surface currents and H-field going in these directions. The absorbing material that were applied is called Eccosorb MSC and is effective up to $18\,\mathrm{GHz}$. This added some loss and lower the efficiency of the antenna. Eccosorb was added along the right, left and top edge, and at the flat edge of the slot between the added taps as shown in fig 5.8.

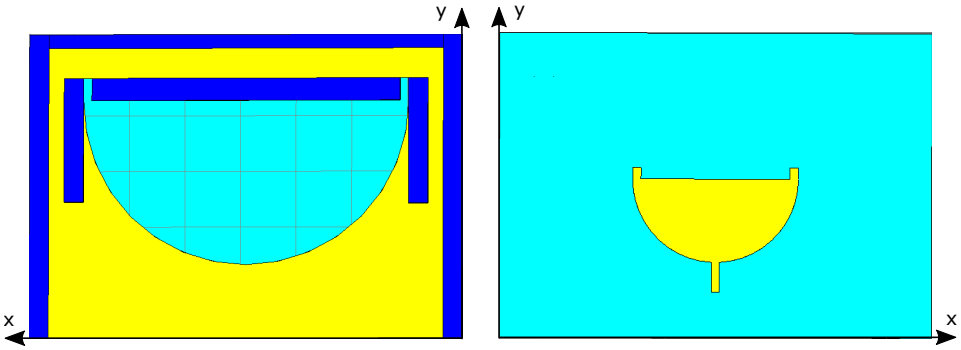

Figure 5.8: Model of the antenna with added taps and eccosorb MSC from CST

The Eccosorb at the right and left side of the slot, as shown in figure 5.8, was added to attenuate the travelling wave going in the direction of the black arrows and avoid the wave from going backwards or out to the edges and along the flat edge of the slot at higher frequencies. In figure 5.11, 5.12, 5.13 and 5.14 the E-plane and H-plane patterns for 3.5 and $6\,\mathrm{GHz}$ are compared with and without Eccosorb MSC. We can see in figure 5.11 that

we remove a deep notch in the E-plane pattern at 3.5 GHz, and in figure 5.12 that the ripple is not as deep as it was without Eccosorb MSC in the design. It is also good to see that there are less deep ripples in the H-plane pattern at 6 GHz as shown in figure 5.14.

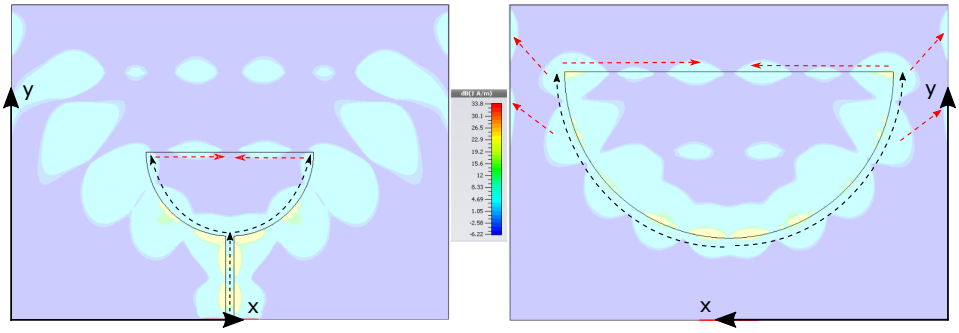

Figure 5.9: Surface currents at 6 GHz simulated in CST

The radiation efficiency of the design with and without absorbent is shown in figure 5.10. The absorbent will attenuate the travelling wave and add some loss to the design.

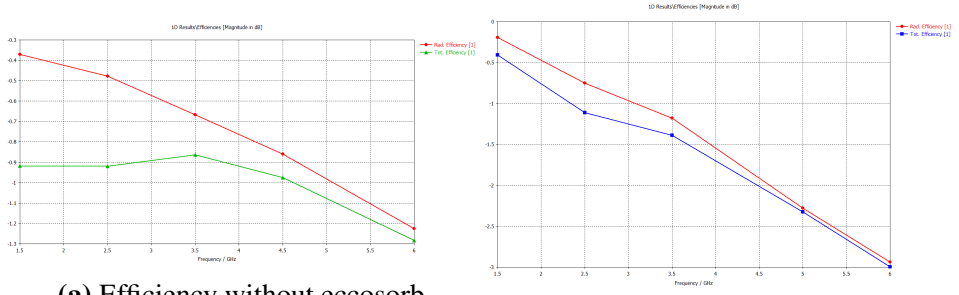

(a) Efficiency without eccosorb

(b) Efficiency with eccosorb

Figure 5.10: Comaprison of efficiency with and without eccosorb simulated in CST

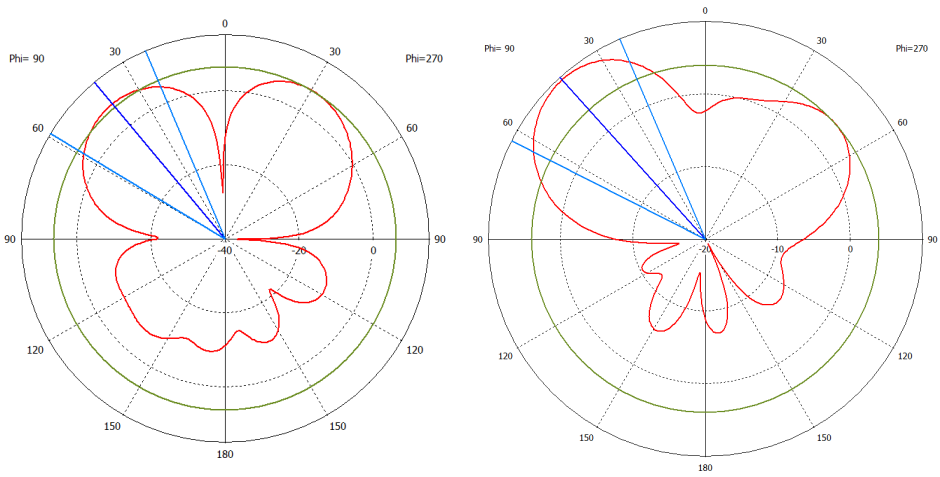

(a) Without Eccosorb **(b)** With Eccosorb

Figure 5.11: Plot of E-plane at 3.5 GHz simulated in CST

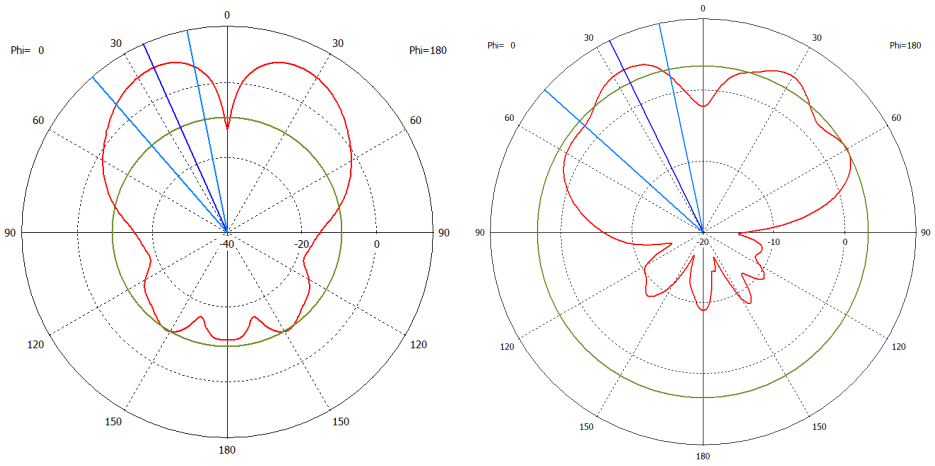

(a) Without Eccosorb **(b)** With Eccosorb

Figure 5.12: Plot of H-plane at 3.5 GHz simulated in CST

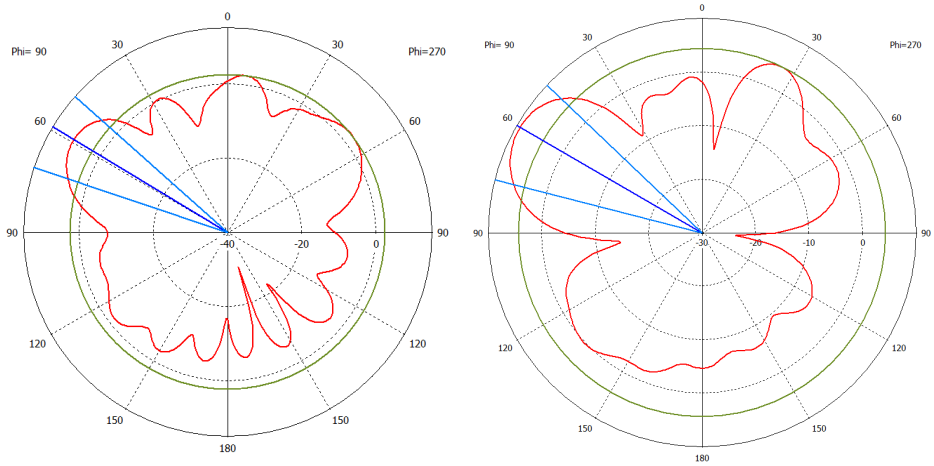

(a) Without Eccosorb **(b)** With Eccosorb

Figure 5.13: Plot of E-plane at 6 GHz simulated in CST

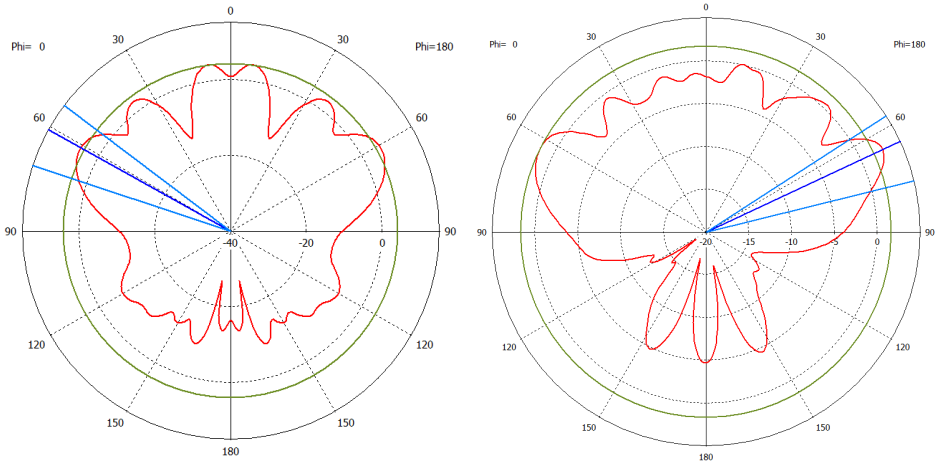

(a) Without Eccosorb **(b)** With Eccosorb

Figure 5.14: Plot of H-plane at 6 GHz simulated in CST

5.5 Antenna element design

The described steps in this chapter led to a design that was sufficient for the specifications and this design was not further developed. This section will give a detailed sketch of the antenna with dimensions and important plots for the different parameters. The antenna was made on a $1.6\,\mathrm{mm}$ FR4 substrate with $\epsilon \approx 4.6$, $\tan\delta \approx 0.015$ and the copper layer on both sides has a thickness of approximately $36\,\mu\mathrm{m}$.

5.5.1 Design with dimensions

An illustration of the designed antenna is shown in figure 5.15 with the most important dimensions displayed. Another important parameter is the gap between the slot and the radiating patch on the front. The gap is $0.5\,\mathrm{mm}$ and is important for the coupling between the two layers. The SMA-connector is placed $17.1\,\mathrm{mm}$ from the bottom edge. The size of the antenna is $156\mathrm{mm} \times 109.2\mathrm{mm}$. The added holes at in the four corners of the antenna had a diameter of $4\,\mathrm{mm}$ and were added to be able to screw the antenna to the divinycell and reflector plate. The simulations in this chapter includes the holes in all these layers and a plastic screw through the holes.

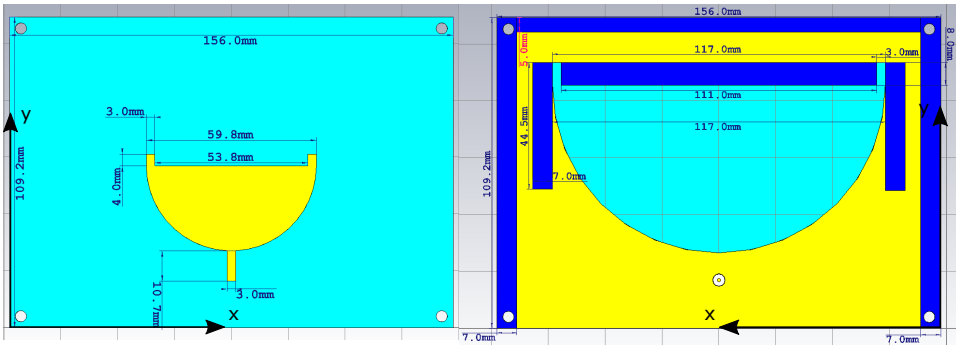

Figure 5.15: Illustration of the designed antenna with dimensions

5.5.2 S-parameters, bandwidth and efficiency

The S-parameter plot was analyzed to see at which frequencies the antenna radiates and how much energy that is radiated. In figure 5.16 we can see that the antenna has a bandwidth ranging from $1.45\,\mathrm{GHz}$ and above the specified upper frequency of $6\,\mathrm{GHz}$. As previously discussed, $S_{1,1}$ below $-10\,\mathrm{dB}$ is the limit and even lower values are even better.

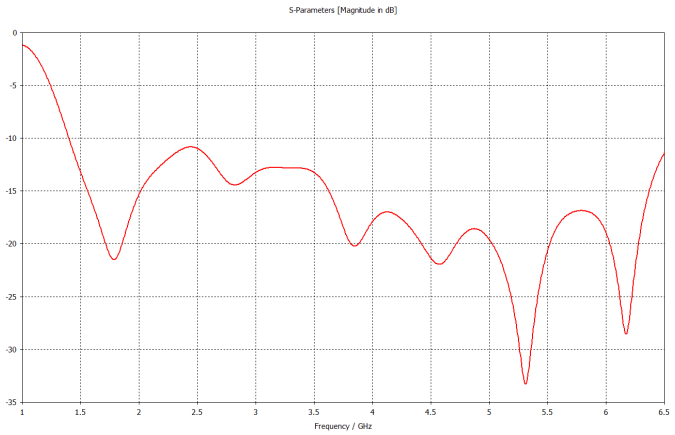

Figure 5.16: Simulated S-parameter for the complete design from CST

5.5.3 E-plane and H-plane

The plots of E-plane and H-plane are presented in figures 5.17, 5.18, 5.19, 5.20 and 5.21. The orientation of the two planes is as shown in figure 5.1.

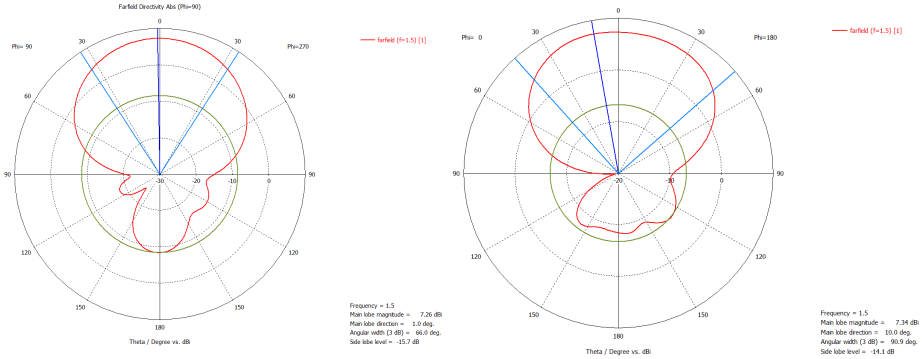

(a) E-plane at 1.5 GHz

(b) H-plane at 1.5 GHz

Figure 5.17: E-plane and H-plane at 1.5 GHz simulated in CST

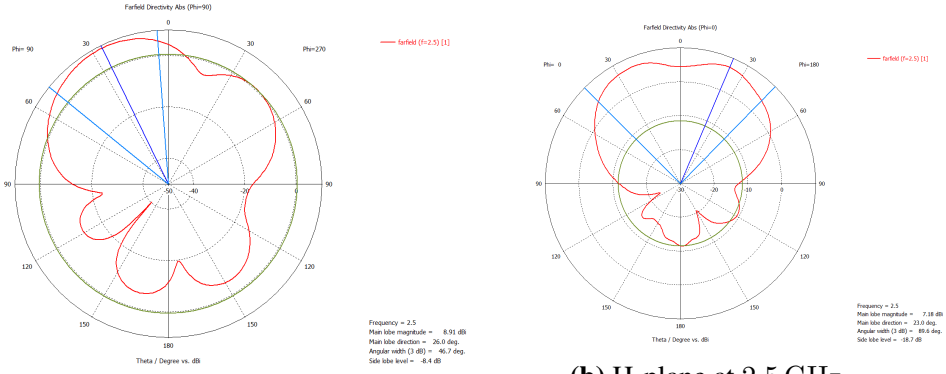

(a) E-plane at 2.5 GHz

(b) H-plane at 2.5 GHz

Figure 5.18: E-plane and H-plane at 2.5 GHz simulated in CST

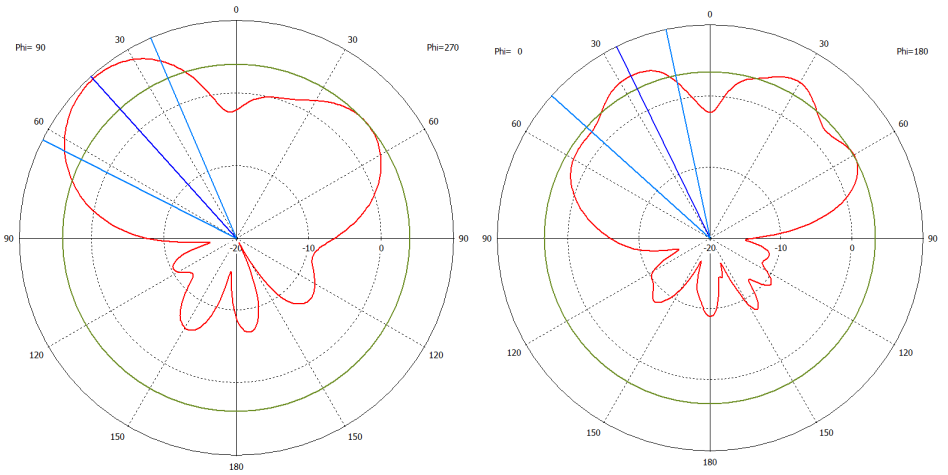

(a) E-plane at 3.5 GHz **(b)** H-plane at 3.5 GHz

Figure 5.19: E-plane and H-plane at 3.5 GHz simulated in CST

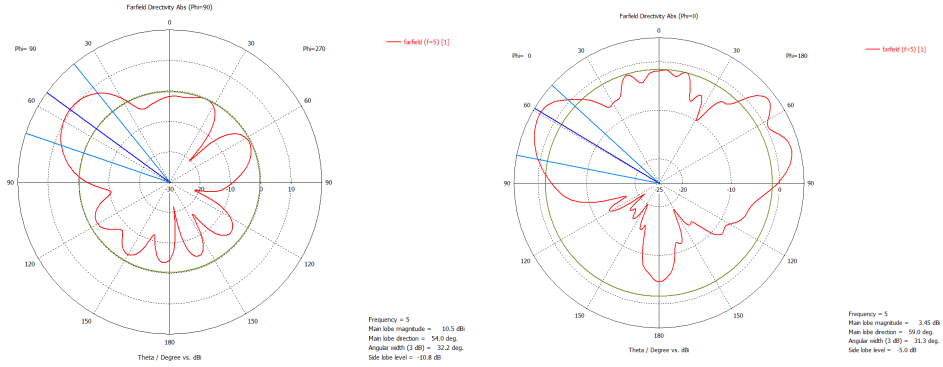

(a) E-plane at 5 GHz **(b)** H-plane at 5 GHz

Figure 5.20: E-plane and H-plane at 5 GHz simulated in CST

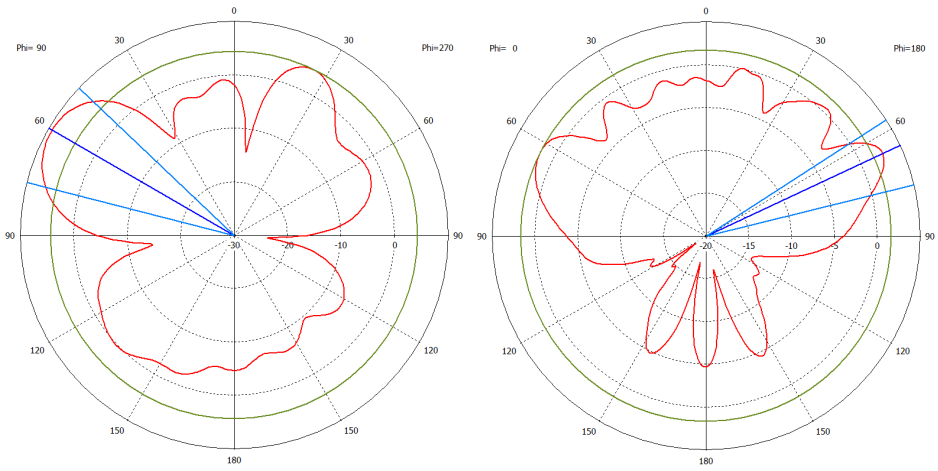

(a) E-plane at 6 GHz **(b)** H-plane at 6 GHz

Figure 5.21: E-plane and H-plane at 6 GHz simulated in CST

5.6 Array of two elements

The idea of this project was to fit as many antennas that fulfilled the specifications from table 2.1 on a $12\,\mathrm{cm}$ times $30\,\mathrm{cm}$ panel, and to place 16 of these panels in a cylinder as shown in figure 2.1. With the size of the antenna there would only be space for 2 elements and there would also be an increase of the size of the panels by a few cm. According to section 4.2 the spacing between the two elements in the array should be less or equal to $\frac{5*\lambda}{6}$ which translates to a distance at $41.67\,\mathrm{mm}$ for $6\,\mathrm{GHz}$ and $69.16\,\mathrm{mm}$ for the center frequency ($3.6\,\mathrm{GHz}$). With the size of the antenna this is not possible to do in the same plane. The two elements were placed as close as possible with a gap of $4\,\mathrm{mm}$ to avoid unwanted coupling effects between the two elements. The spacing of the centers of the elements ended up being d = $160\,\mathrm{mm}$ as shown in figure 5.22. The size of a single plate was at this point $12.5\,\mathrm{cm}$ times $40\,\mathrm{cm}$. In figure 5.23 the S-parameter results for a 2-port simulation of the array is presented. We can see that $S_{2,1}$ and $S_{1,2}$ is quite high for the lower frequencies of the bandwidth and the elements will have strong coupling at frequencies lower than $2\,\mathrm{GHz}$. $S_{1,1}$ is still lower than $-10\,\mathrm{dB}$ from around $1.4\,\mathrm{GHz}$ and above $6\,\mathrm{GHz}$.

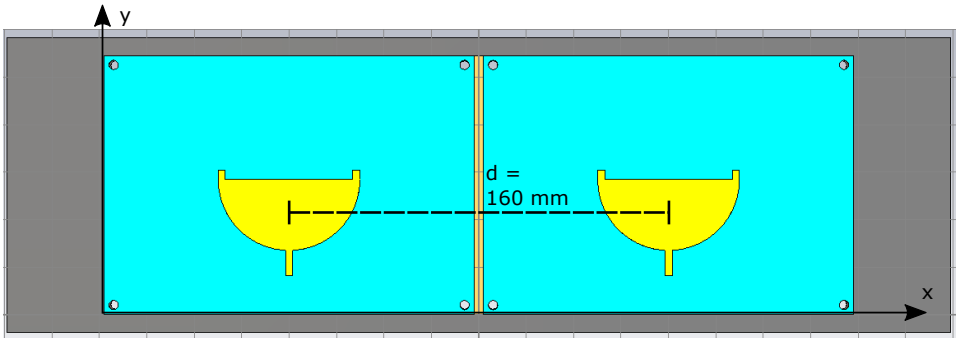

Figure 5.22: Illustration of the array setup with element distance d = 160 mm

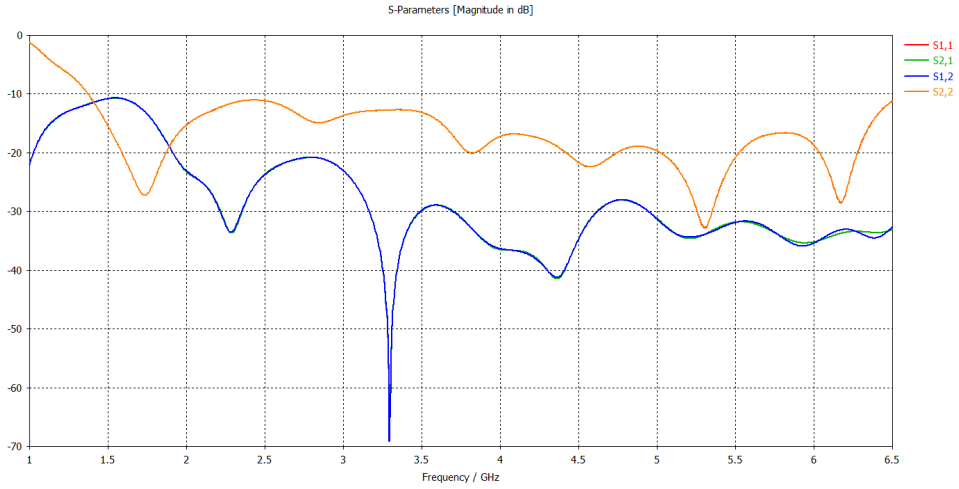

Figure 5.23: S-parameters for the array of two elements from CST

5.6.1 H-plane for the array of two elements

In figures 5.24, 5.25 and 5.26 the simulation results for the H-plane is presented. The main lobe gets more and more narrow at higher frequencies with multiple side lobes. The plots of the E-plane is not included because the array factor only affects the H-plane. The E-plane will experience any effect of the array.

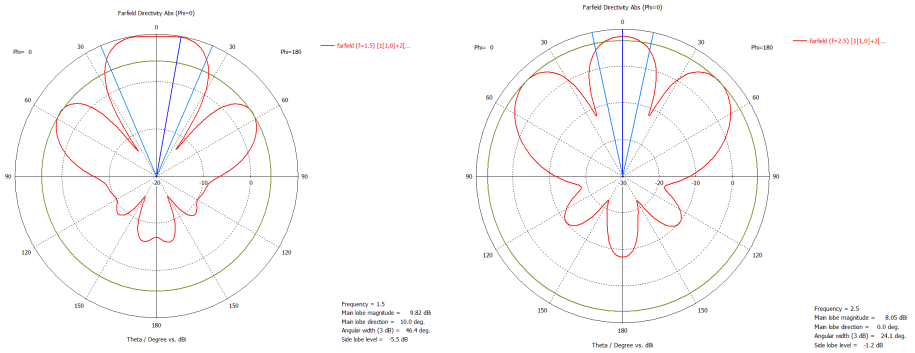

Figure 5.24: H-plane for the two element array at 1.5 GHz and 2.5 GHz simulated in CST

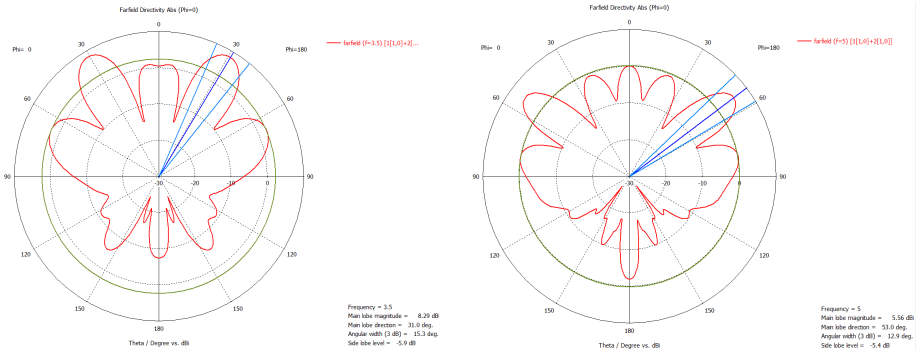

Figure 5.25: H-plane for the two element array at 3.5 GHz and 4.5 GHz simulated in CST

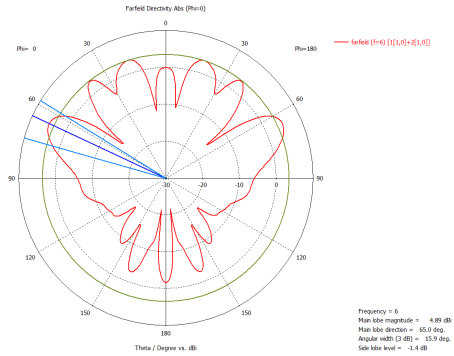

Figure 5.26: H-plane for the two element array at 6 GHz simulated in CST

Chapter 6

Experimental results

This chapter will present the results from measurement of the antenna formed in this thesis according to the design found in chapter 5.5. The results will only be presented in this chapter, and in the next chapter be discussed and compared to the simulation results. The antenna was tested in an antenna lab at NTNU where an ANA and an anechoic chamber is found giving results for S-parameter, E-plane and H-plane. The design was etched with laser and the port was soldered to the feed in the front and to the metal at the backside as shown in figure 6.1. There was a hole for the inner conductor of the port through the antenna, and the inner conductor was soldered to the feed as seen in figure 6.1a.

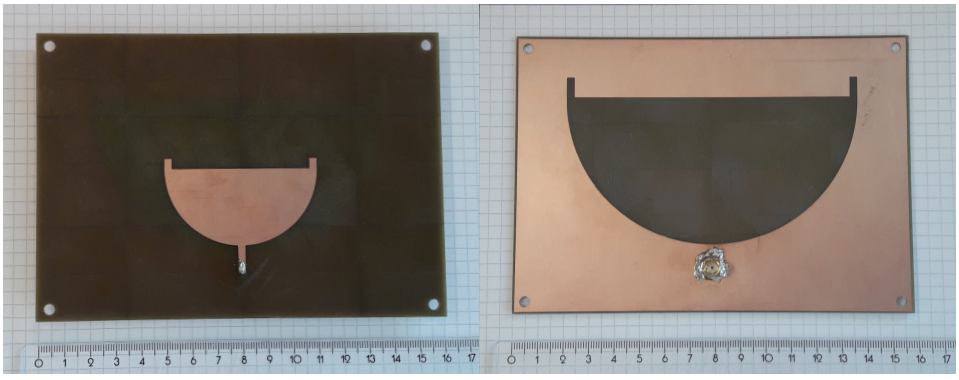

(a) Front of the antenna **(b)** Backside of the antenna

Figure 6.1: The manufactured antenna that was tested

6.1 S-parameter

To measure the S-parameter an ANA (HP 8720B) was calibrated and the antenna was connected to port 1. As discussed earlier, when we measure $S_{1,1}$ we measure how much of the power applied to port 1 that is reflected. Since this circuit or antenna only has 1 port, the power that is not reflected must be radiated or attenuated by the antenna. We want $S_{1,1}$ to have as low value as possibly to assure that the antenna radiates most of the power applied to it.

In figure 6.2 and 6.3 we find $S_{1,1}$ plotted for the antenna without reflector plate and the antenna with reflector plate respectively. The result for a single antenna without reflector plane gives the antenna a $S_{1,1}$ with values below $-10\,\mathrm{dB}$ from $560\,\mathrm{MHz}$ to $8.7\,\mathrm{GHz}$ and from $1.2\,\mathrm{GHz}$ to $8.7\,\mathrm{GHz}$ for the measurement with reflector plate (6.3).

When the bandwidth is known, it is easy to calculate the Q-factor for the antenna with the formula from section 4.5.

$$Q = \frac{f_c}{f_{max} - f_{min}} = 0.66$$

The Q-factor is dimensionless and tells us about the loss and energy storage properties for the antenna. With a quality factor above 0.5 we can say that the antenna is underdamped and the signal might oscillate a few times before dying out.

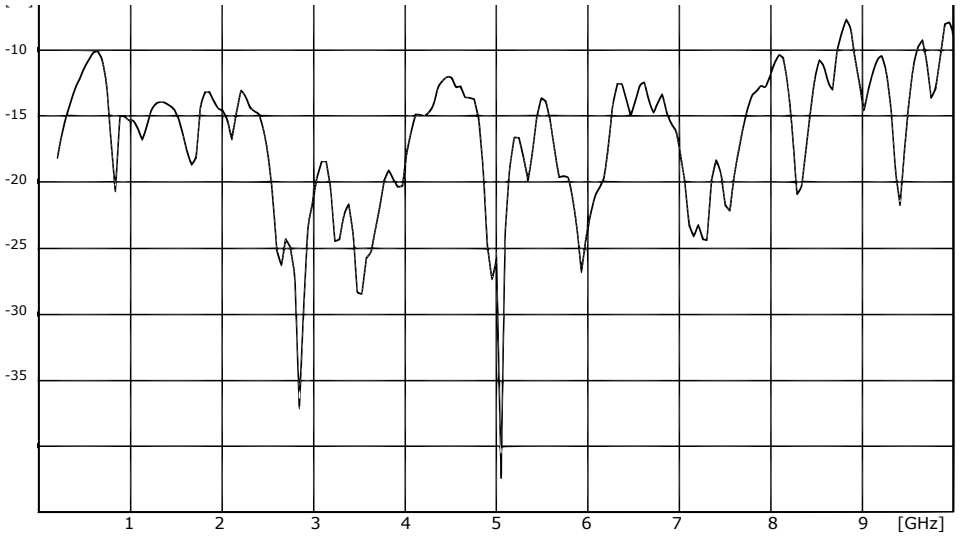

Figure 6.2: $S_{1,1}$ for 200 MHz to 10 GHz measured with HP 8720B without reflector and divinycell plate

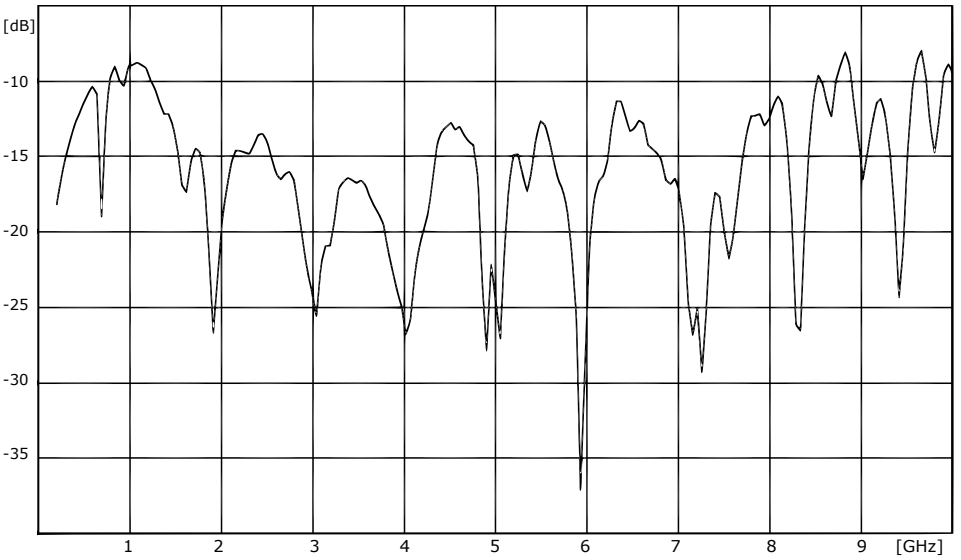

Figure 6.3: $S_{1,1}$ for 200 MHz to 10 GHz measured with HP 8720B with reflector and divinycell plate

6.2 E-plane radiation pattern

The results of E-plane pattern are illustrated in the figure 6.4 to 6.9 in this section. These measurements were done in the antenna lab at NTNU as described in chapter 4.4.4. The pattern is made from the values for $S_{2,1}$ from an anechoic chamber where an ultra-wideband horn is connected to port 1, and the antenna under test to port 2 and $S_{2,1}$ denotes how much power that is received from the horn antenna at port 1. These tests were performed without absorbents as illustrated in section 5.5.

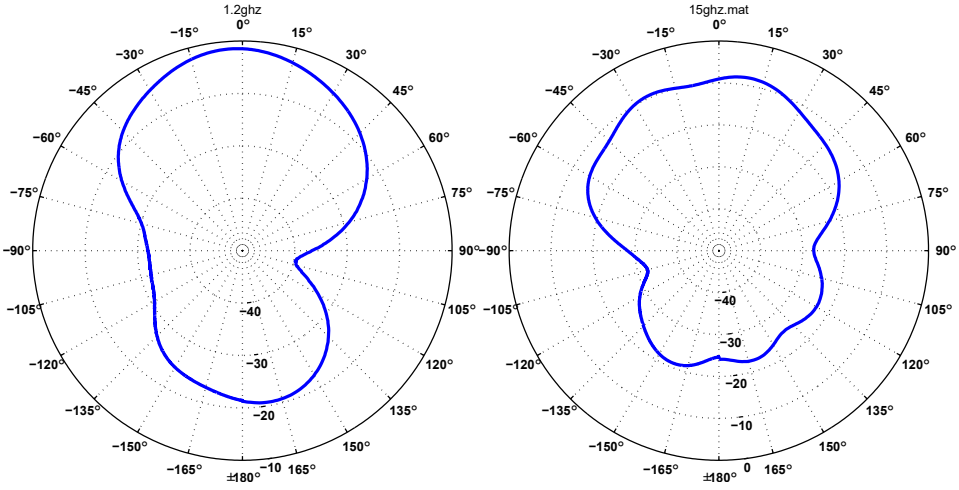

(a) E-plane at 1.2 GHz **(b)** E-plane at 1.5 GHz

Figure 6.4: E-plane at 1.2 GHz and 1.5 GHz measured in an anechoic chamber

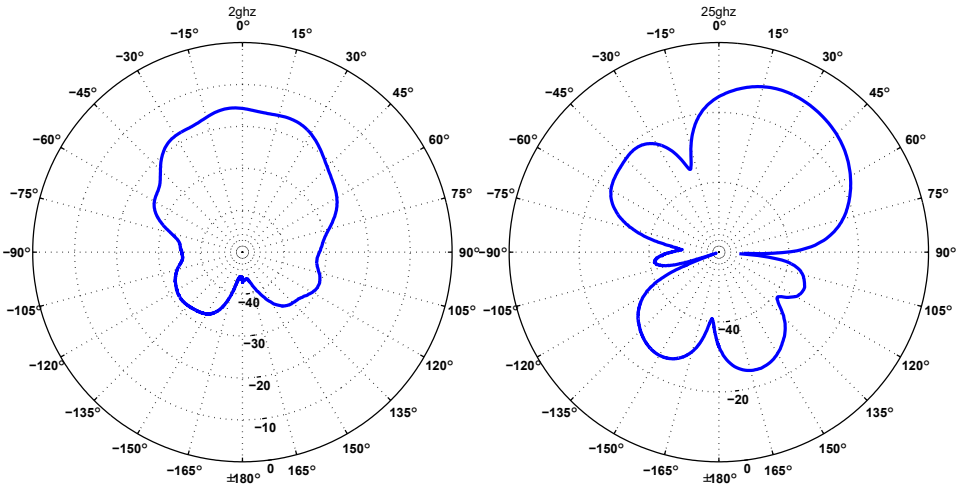

(a) E-plane at 2 GHz **(b)** E-plane at 2.5 GHz

Figure 6.5: E-plane at 2 GHz and 2.5 GHz measured in an anechoic chamber

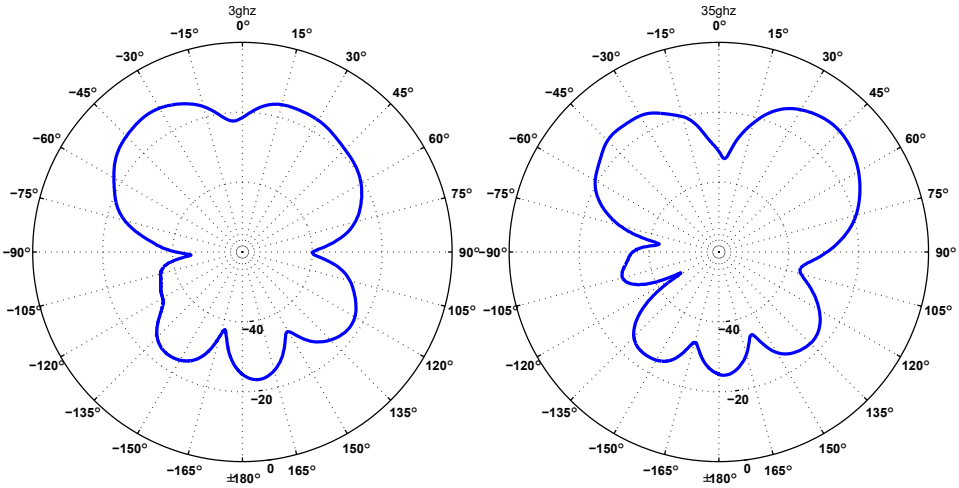

(a) E-plane at 3 GHz **(b)** E-plane at 3.5 GHz

Figure 6.6: E-plane at 3 GHz and 3.5 GHz measured in an anechoic chamber

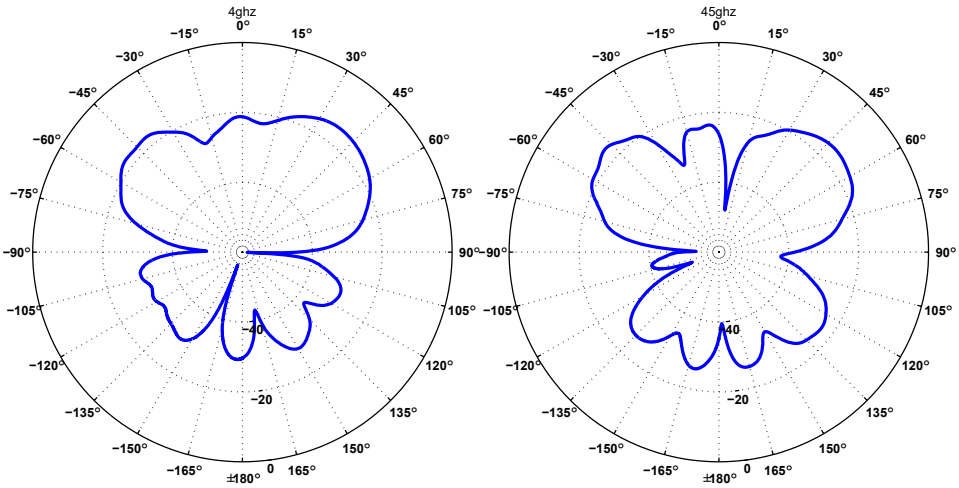

(a) E-plane at 4 GHz **(b)** E-plane at 4.5 GHz

Figure 6.7: E-plane at 4 GHz and 4.5 GHz measured in an anechoic chamber

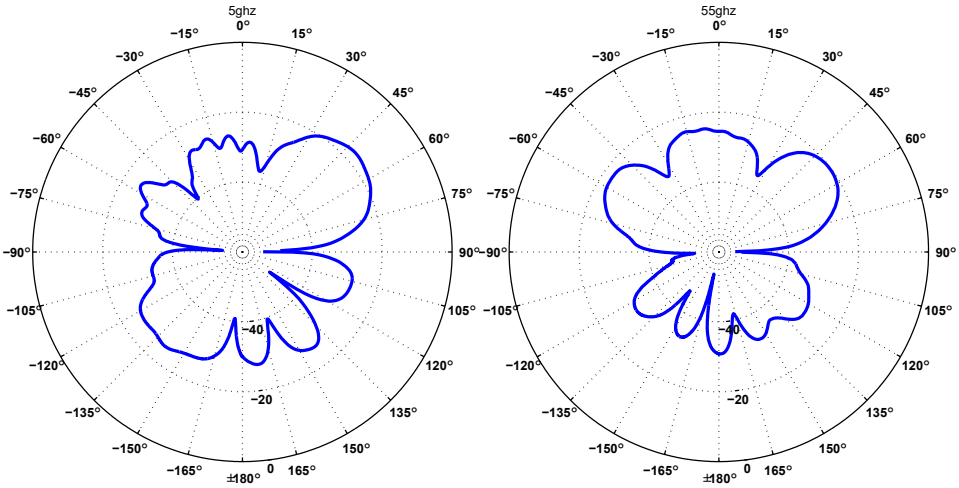

(a) E-plane at 5 GHz **(b)** E-plane at 5.5 GHz

Figure 6.8: E-plane at 5 GHz and 5.5 GHz measured in an anechoic chamber

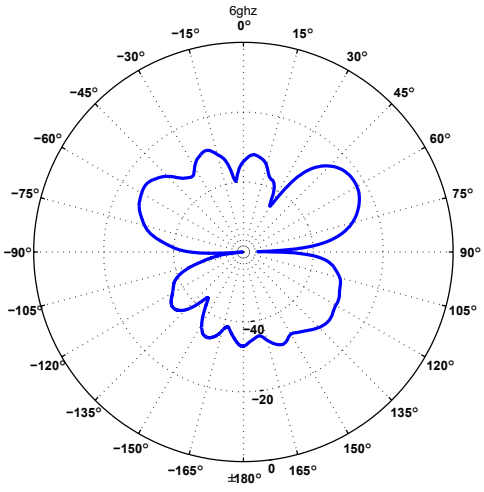

Figure 6.9: E-plane at 6 GHz

6.3 H-plane radiation pattern

This section presents the results for the H-plane and were gathered as described in the previous section. Both the slot antenna and the horn antenna were rotated $90°$ to obtain results for the H-plane. The results are shown in figure 6.10 to 6.15 and will be discussed in the next chapter.

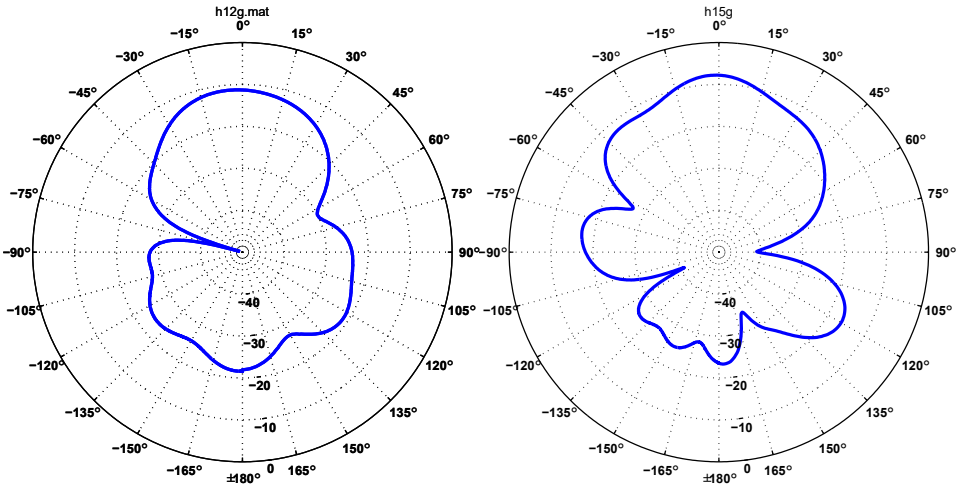

(a) H-plane at 1.2 GHz **(b)** H-plane at 1.5 GHz

Figure 6.10: H-plane at 1.2 GHz and 1.5 GHz measured in an anechoic chamber

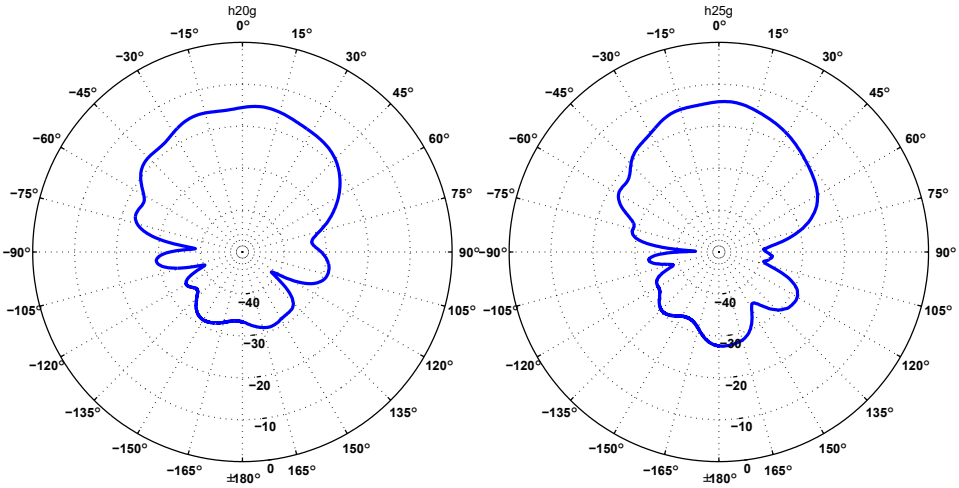

(a) H-plane at 2 GHz **(b)** H-plane at 2.5 GHz

Figure 6.11: H-plane at 2 GHz and 2.5 GHz measured in an anechoic chamber

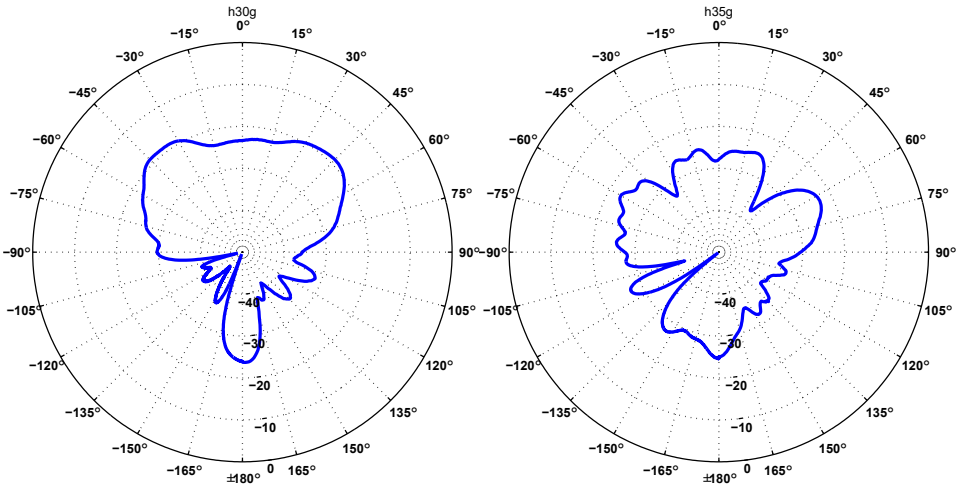

(a) H-plane at 3 GHz **(b)** H-plane at 3.5 GHz

Figure 6.12: H-plane at 3 GHz and 3.5 GHz measured in an anechoic chamber

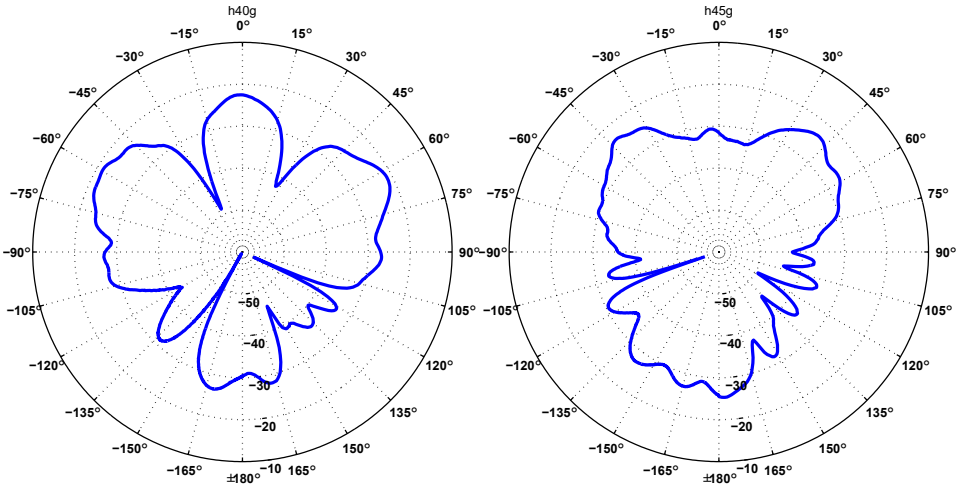

(a) H-plane at 4 GHz **(b)** H-plane at 4.5 GHz

Figure 6.13: H-plane at 4 GHz and 4.5 GHz measured in an anechoic chamber

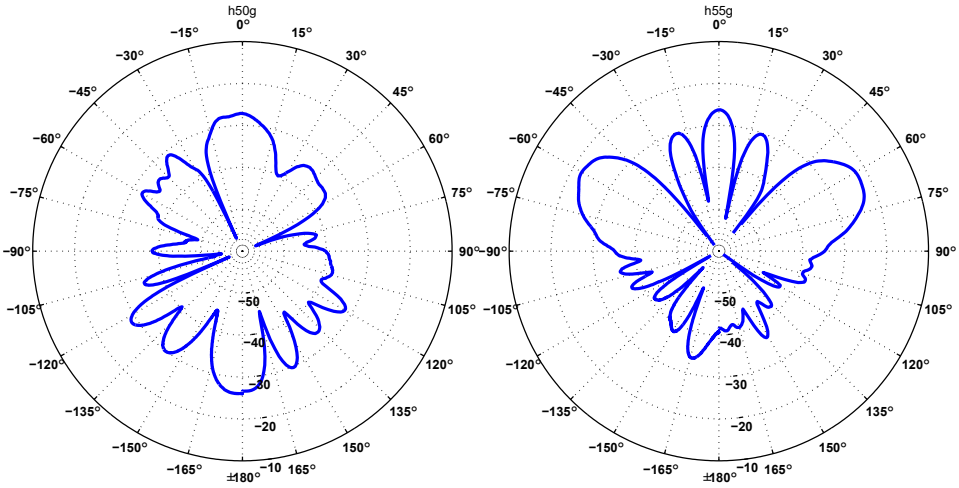

(a) H-plane at 5 GHz **(b)** H-plane at 5.5 GHz

Figure 6.14: H-plane at 5 GHz and 5.5 GHz measured in an anechoic chamber

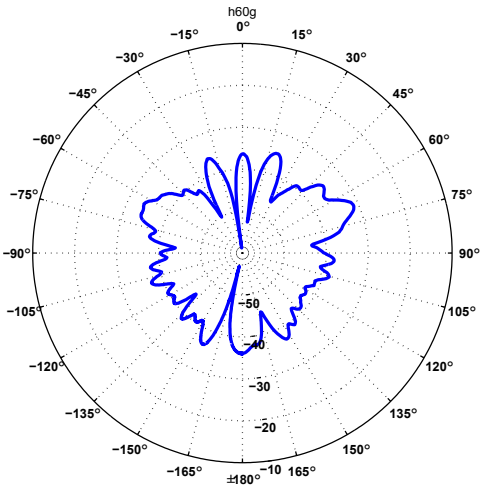

Figure 6.15: H-plane at 6 GHz

6.4 Polarization

The polarization was already known from the simulations but a simple test were performed to verify these results. A horn antenna as described in the above sections were used and has a known polarization. The E-plane tests were done as described in section 6.2 and then the antenna was rotated $90°$. There was a large difference in received power when the results of the two tests were compared. The difference in received power from horizontal and vertically excited radiation was around $-20\,\mathrm{dB}$ when the antennas were pointing directly at each other. With the orientation of the antenna as shown in chapter 5 the planes were oriented as the figure illustrates and is also what was expected from simulations and from a qualified guess. With the orientation from figure 5.1 the antenna has a horizontal linear polarization.

Chapter 7

Discussion

This chapter will mainly compare and discuss the results from simulations and the results from measurements. A comparison between the specifications and the obtained results will also be found in this chapter.

7.1 Specifications

In this section the results and specifications will be compared and discussed. All through the process of this design and this thesis the goal has been to fulfill the specification from table 2.1.

Bandwidth The goal was to get a bandwidth from $800\,\mathrm{MHz}$ to $6\,\mathrm{GHz}$. The final design had a bandwidth ranging from $1.2\,\mathrm{GHz}$ to $8.7\,\mathrm{GHz}$ when analyzing the s-parameters. The E-plane and H-plane has to much ripple at frequencies above $2.5\,\mathrm{GHz}$. The bandwidth, according to $S_{1,1}$, was in the range from $560\,\mathrm{MHz}$ to $8.7\,\mathrm{GHz}$ without the reflector plate which is more than the specified bandwidth.

Polarization It was specified that the antenna should have a linear polarization and it was not specified if it should be horizontal or vertical. From the results and simulations it was found that the antenna is linear horizontal polarized.

Size The size of the base station setup, which should be a cylinder with multiple antennas, was specified to have a radius and height equal to or less than $30\,\mathrm{cm}$. The idea was to make 16 equal panels with the equal amount of antenna elements on each panel. These panels would then have to be at the size of $12\,\mathrm{cm}$ by $30\,\mathrm{cm}$, and ended up being $12.5\,\mathrm{cm}$ by $40\,\mathrm{cm}$. This will make a cylinder with a radius equal to $32\,\mathrm{cm}$ and height of $40\,\mathrm{cm}$.

Radiation Pattern The radiation pattern are sufficient when the antenna operates as an monopole and for frequencies up to $2.5\,\mathrm{GHz}$. When the antenna operates as a travelling wave antenna the E-plane radiation pattern tilts and is not directly in the positive z-direction. The half circle shape is considered small compared to the wave length at lower frequencies, but at higher frequencies will the distance between the two edges and the two waves propagating on the them be considered as large and the radiations pattern will get some ripple. The distance between the two waves adds an array effect to the single element and adds a lot of ripple when the frequency gets higher.

Array setup The element distance is to large and the array does not perform as wanted. The main lobe is narrow and the radiation pattern for the H-plane have multiple side lobes. As the frequency gets higher, the main lobe gets more narrow and the number of side lobes gets higher.

The frequencies lower than $1.2\,\mathrm{GHz}$ was not covered by the antenna, with the reflector plate, and the reason is the size constraints in the specifications. The design did exceed the size specifications by a few cm to include some of the lower frequencies in the bandwidth. The radius of the cylinder was not far from the specifications, but the cylinder will be $10\,\mathrm{cm}$ higher than specified. It is possible to install one antenna per panel and decrease the height or reduced the number of panels to reduce the radius of the cylinder.

7.2 E-plane radiation pattern

Figure 7.1, 7.2, 7.3, 7.4 and 7.5 shows that the measured and simulated results are quite similar. The measured beam patterns have a wide mainlobe in the positive z-direction as wanted. At higher frequencies, we get a deep notch as shown in figure 7.2, 7.3 and 7.4 and the notch is also found in all the plots of the E-plane at frequencies higher than $2\,\mathrm{GHz}$ from chapter 5 and 6. There is a lot of ripple in the measured and simulated pattern at $6\,\mathrm{GHz}$ as seen in figure 7.5. In the simulations an absorbent was added to minimize this effect and to suppress the notch. This helped in the simulations but were not tested by measurements.

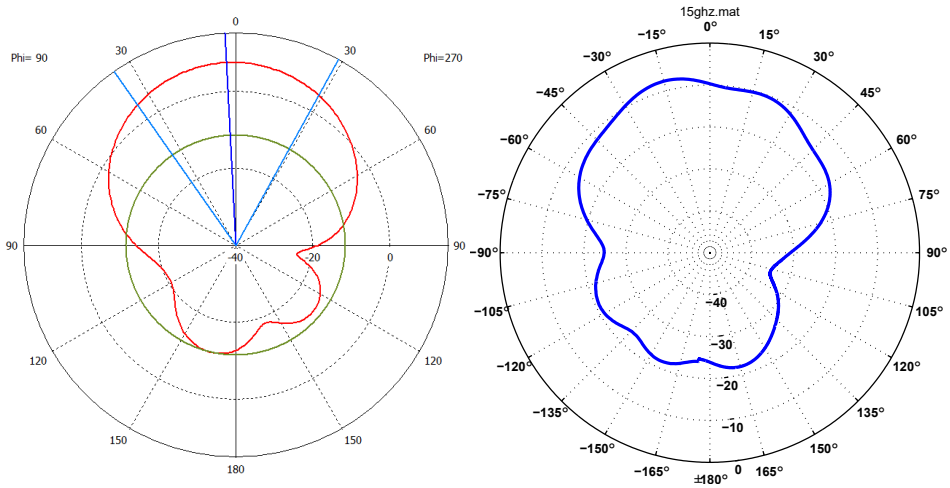

(a) Simulated E-plane at $1.5\,\mathrm{GHz}$ **(b)** Measured E-plane at $1.5\,\mathrm{GHz}$

Figure 7.1: Comparison of the simulated and measured E-plane at $1.5\,\mathrm{GHz}$

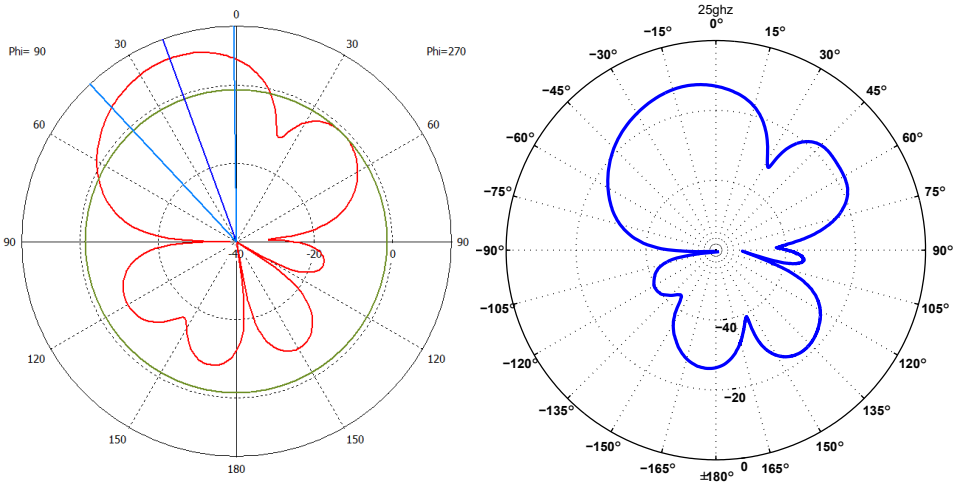

(a) Simulated E-plane at 2.5 GHz **(b)** Measured E-plane at 2.5 GHz

Figure 7.2: Comparison of the simulated and measured E-plane at 2.5 GHz

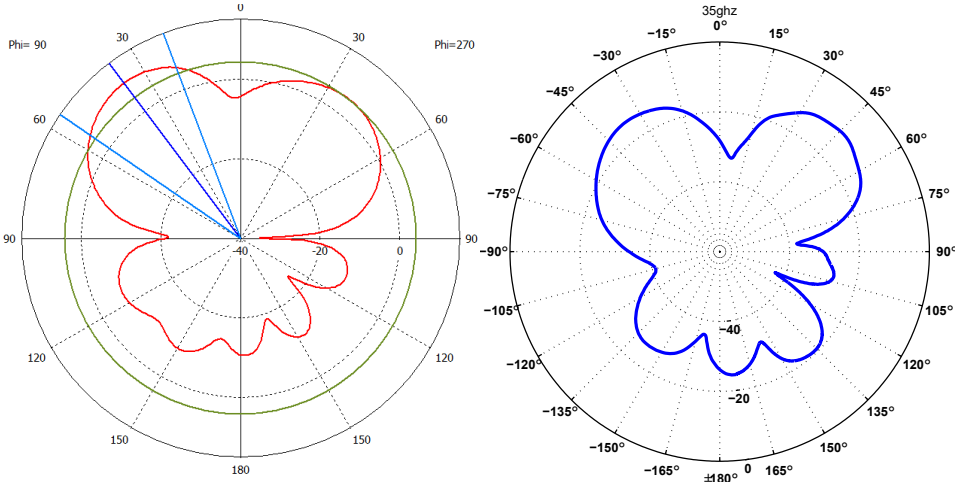

(a) Simulated E-plane at 3.5 GHz **(b)** Measured E-plane at 3.5 GHz

Figure 7.3: Comparison of the simulated and measured E-plane at 3.5 GHz

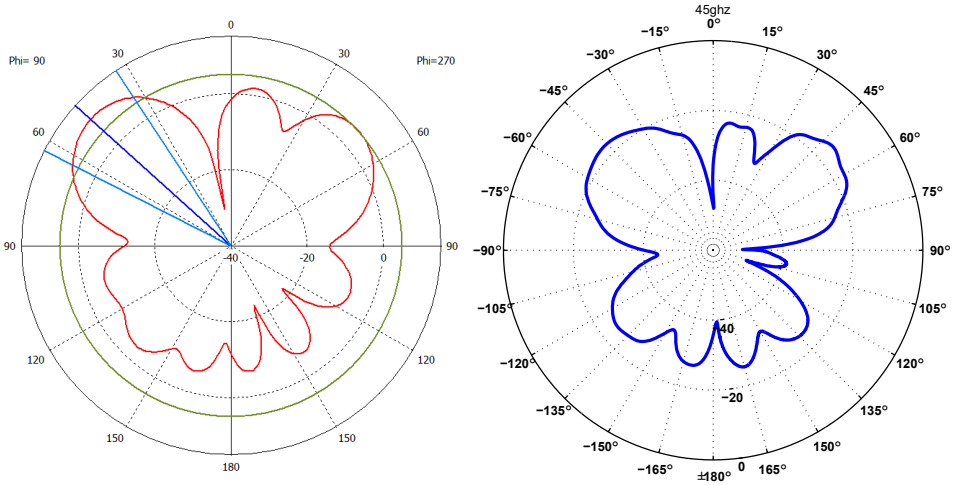

(a) Simulated E-plane at 4.5 GHz **(b)** Measured E-plane at 4.5 GHz

Figure 7.4: Comparison of the simulated and measured E-plane at 4.5 GHz

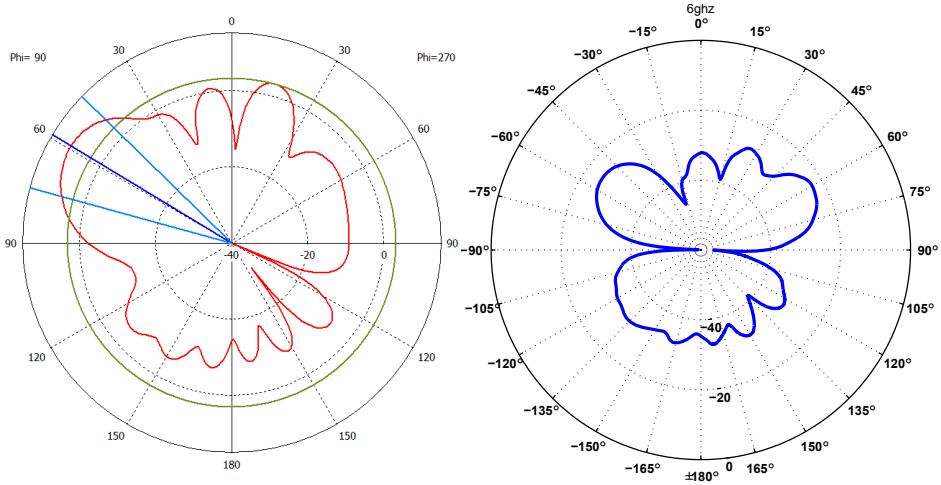

(a) Simulated E-plane at 6 GHz **(b)** Measured E-plane at 6 GHz

Figure 7.5: Comparison of the simulated and measured E-plane at 6 GHz

7.3 H-plane radiation pattern

The simulated and measured results for the H-plane have some similarities but differs more than the results for the E-plane. The comparison of the results from simulations and measurements are found in figure 7.6, 7.7, 7.8, 7.9 and 7.10. The main reason for the differences might be that in simulations the reflector plate was made of Perfect Electric Conductor (PEC) which have different magnetic properties than aluminum that was used as a reflector plate. The performance of the antenna would probably be better with the absorbent, but was not tested by measurements. The missing absorbent does not affect the similarity because both the simulated and measured results is without the absorbent. The scaling of the polar plot axis might make the measured pattern less distinct. But there are similarities in the plots in figure 7.6, 7.7 and 7.9 which presents the simulated and measured H-plane at $1.5\,\text{GHz}$, $2.5\,\text{GHz}$ and $4.5\,\text{GHz}$.

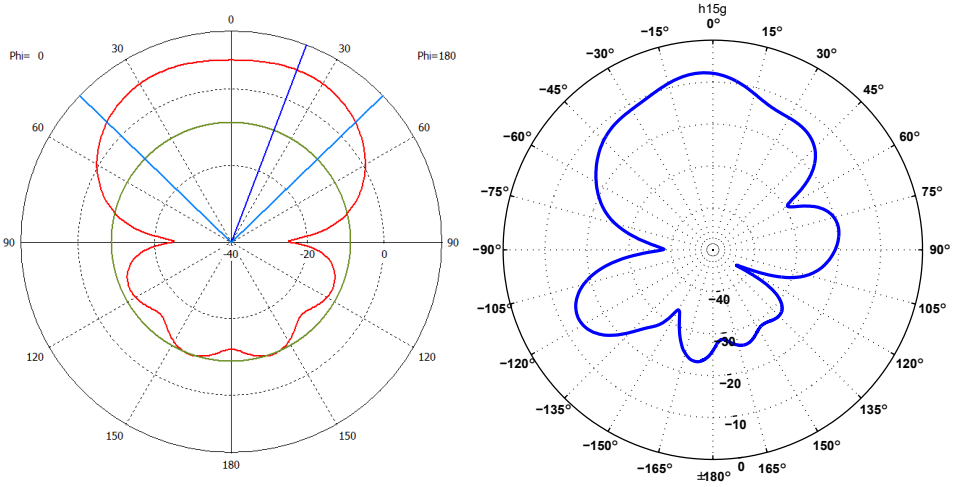

(a) Simulated H-plane at $1.5\,\text{GHz}$ **(b)** Measured H-plane at $1.5\,\text{GHz}$

Figure 7.6: Comparison of the simulated and measured H-plane at $1.5\,\text{GHz}$

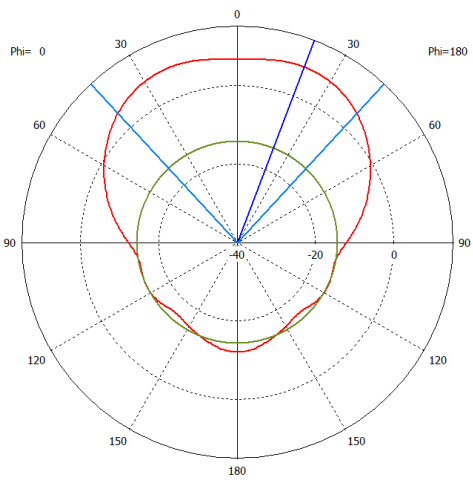

(a) Simulated E-plane at 2.5 GHz

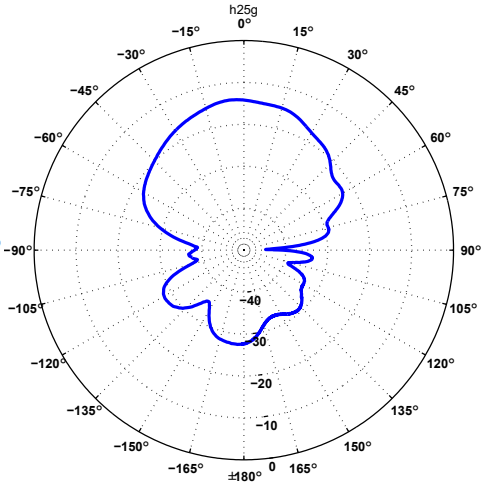

(b) Measured E-plane at 2.5 GHz

Figure 7.7: Comparison of the simulated and measured H-plane at 2.5 GHz

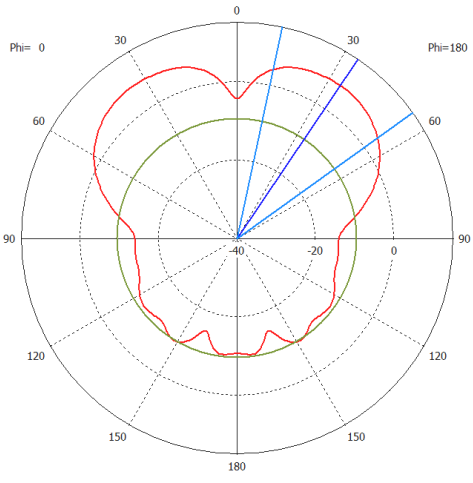

(a) Simulated H-plane at 3.5 GHz

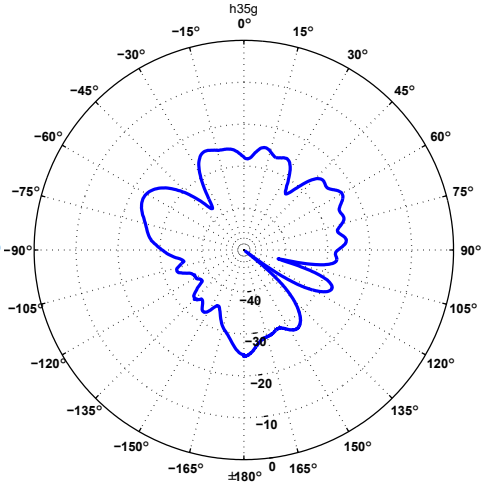

(b) Measured H-plane at 3.5 GHz

Figure 7.8: Comparison of the simulated and measured H-plane at 3.5 GHz

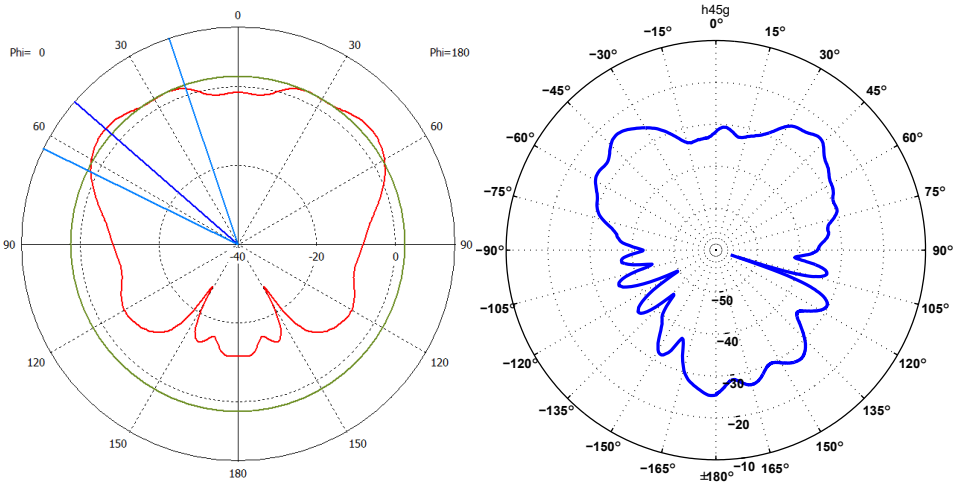

(a) Simulated H-plane at 4.5 GHz **(b)** Measured H-plane at 4.5 GHz

Figure 7.9: Comparison of the simulated and measured H-plane at 4.5 GHz

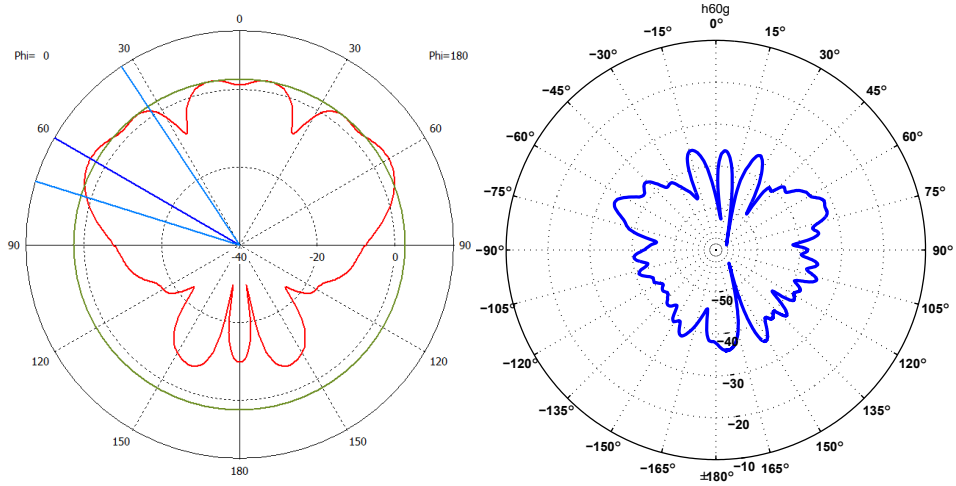

(a) Simulated H-plane at 6 GHz **(b)** Measured H-plane at 6 GHz

Figure 7.10: Comparison of the simulated and measured H-plane at 6 GHz

7.4 Improvements

The missing absorbent might have improved the patterns with deep notches but there might also be other techniques that would improve the performance of the antenna. Adding loss will lower the efficiency of the antenna, but will suppress unwanted surface currents and currents and H-fields in directions that is not wanted. It seems that when the frequency gets above $2.5\,\mathrm{GHz}$ or $3\,\mathrm{GHz}$ the current on the backside (the side with the slot) starts to spread up to the upper edge of the antenna as wanted and then spreads back towards the bottom edge making the split in the E-plane as seen in figure 7.2b, 7.3b and 7.4b. If some loss is added to the upper edge it might suppress these surface currents and minimize this effect. This loss could be added by deploying absorbents as illustrated in section 5.4 or by solder resistors at the upper edge or in the slot between the two layers.

Chapter 8

Conclusion

The purpose of this thesis was to design an ultra-wideband antenna for a massive MIMO setup in a maritime environment. The antenna performs well in the range from $1.2\,\mathrm{GHz}$ to $2.5\,\mathrm{GHz}$ and would possible have better properties from $2.5\,\mathrm{GHz}$ to $6\,\mathrm{GHz}$ if the absorbent from section 5.5 or some other modifications were made.

The simulations of the array setup, with the antenna element formed by this thesis, was not sufficient and were not tested in an anechoic chamber. The main reason was that the size of the antenna was to large to get an optimal distance between the elements.

A limiting factor for this design was the size and form constraints. There are many ”not planar” UWB antenna designs that performs better and are more constant in patterns, gain and will perform better for wideband communication systems. (log-periodic, Vivaldi, horn, etc.) But the antenna formed in this thesis is a good test antenna for the lower LTE bands and Wi-Fi at $2.4\,\mathrm{GHz}$. The measured bandwidth for this antenna is up to $8.7\,\mathrm{GHz}$ from analyzing $S_{1,1}$, but the frequencies out of the specification were not tested.

Bibliography

Aziz, S. Z., Jamlos, M. F., July 2016. Planar antenna with u-shaped slot on radiating patch and conductor-backed plane for uwb applications. In: 2016 International Conference on Computer and Communication Engineering (ICCCE). pp. 57–61.

Balanis, C. A., 2005. Antenna Theory AnalysisS And Design. Wiley-Interscience - John Wilet & Sons, Inc. Publication.

E. G. Larsson, O. E., Tufvesson, F., Marzetta, T. L., February 2014. Massive mimo for next generation wireless systems. IEEE Communications Magazine 52 (2), 186–195.

Lodge, O., 1898. Improvements in syntonized telegraphy without line wires. British Patent Office.

Løvaas, H. D., 2016. 5g architecture: Comparing small-cells, network mimo and massive mimo. ITE, NTNU, Specialization thesis.

Schantz, H. G., Nov 2003. Introduction to ultra-wideband antennas. In: IEEE Conference on Ultra Wideband Systems and Technologies, 2003. pp. 1–9.

Schantz, H. G., April 2004. A brief history of uwb antennas. IEEE Aerospace and Electronic Systems Magazine 19 (4), 22–26.

Tammam, E., Yoshitomi, K., Allam, A., El-Sayed, M., Pokharel, R., Yoshida, K., March 2012. Design and analysis of a compact size planar antenna for uwb applications. In: 2012 6th European Conference on Antennas and Propagation (EUCAP). pp. 2811–2814.

Wang, G. M. Z. W. Y., Yu, Z. Y., May 2010. A novel ultra-wideband planar slot antenna. In: 2010 International Conference on Microwave and Millimeter Wave Technology. pp. 303–305.

Wheeler, H. A., Aug 1959. The radiansphere around a small antenna. Proceedings of the IRE 47 (8), 1325–1331.

Appendix

A - Divinycell plate

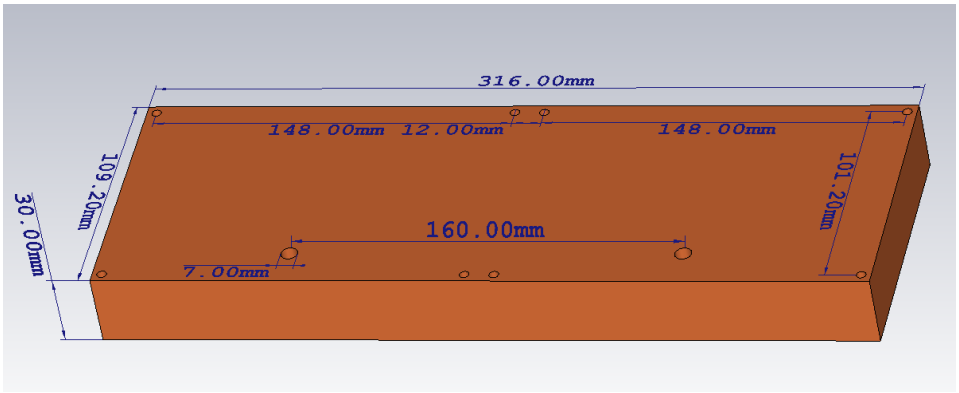

Figure 8.1: Drawing of the divinycell plate from CST

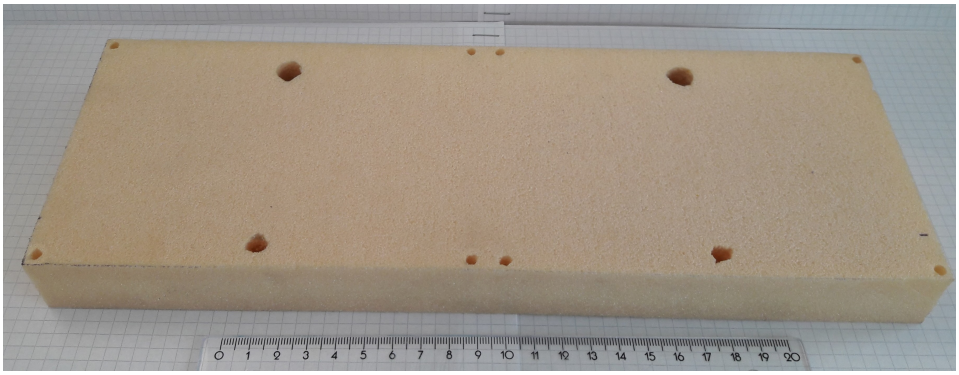

Figure 8.2: Photo of the divinycell plate

B - Reflector plate

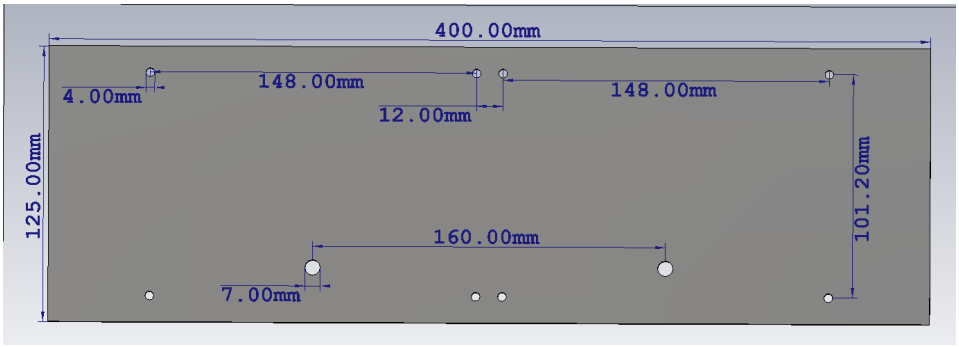

Figure 8.3: Drawing of the reflector plate from CST

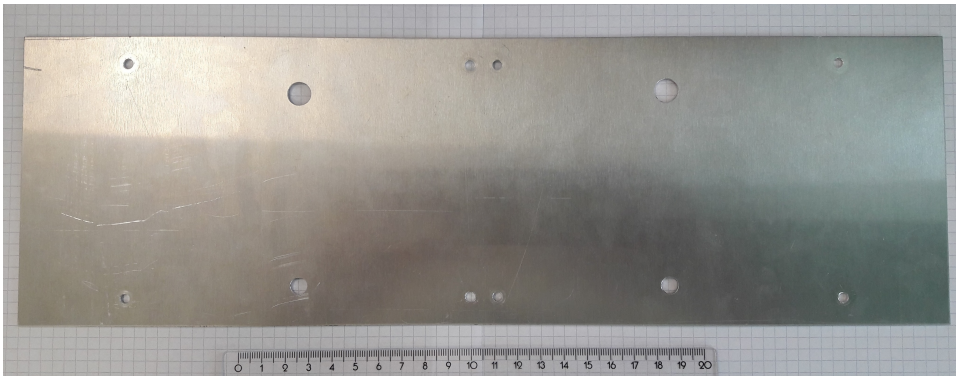

Figure 8.4: Photo of the reflector plate

C - Assembly

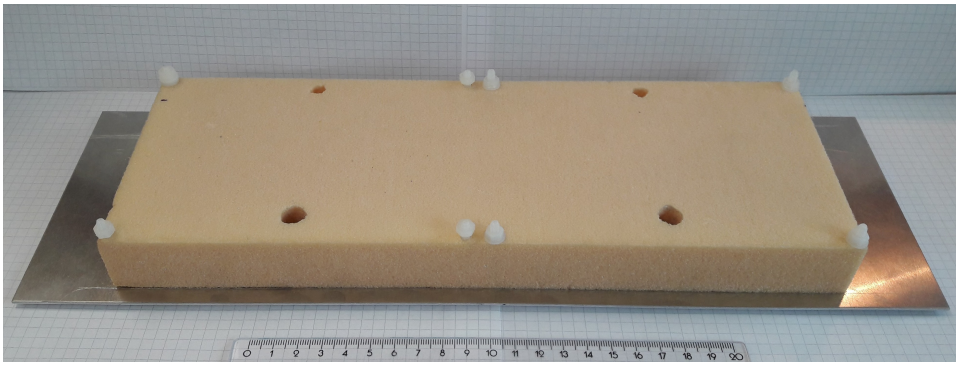

Figure 8.5: Photo of the reflector plate and divinycell plate mounted with $4\,\mathrm{mm}$ plastic screws

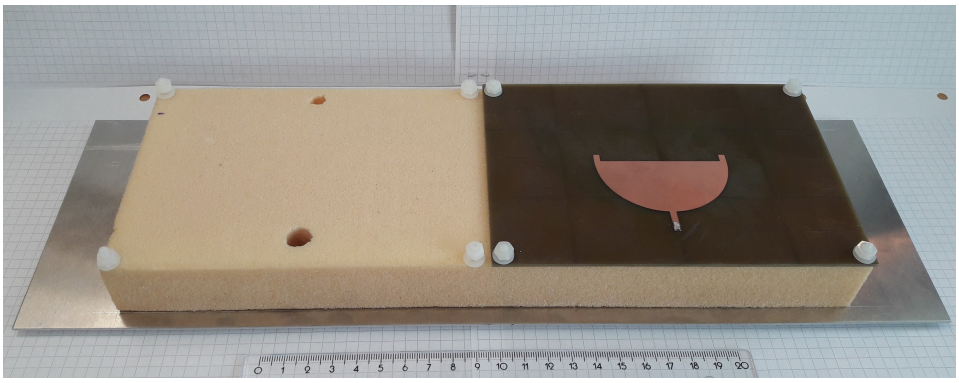

Figure 8.6: Photo of the setup with one antenna